OPTIMIZATION OF OPTICAL PARAMETERS FOR IMPROVED PHOTODYNAMIC THERAPY OF *STAPHYLOCOCCUS AUREUS* USING ENDOGENOUS COPROPORPHYRIN III

By

Alec Bryant Walter

Thesis

Submitted to the Faculty of the

Graduate School of Vanderbilt University

in partial fulfillment of the requirements

for the degree of

MASTER OF SCIENCE

In

Biomedical Engineering

May 10, 2019

Nashville, Tennessee

Approved:

E. Duco Jansen, Ph.D.
Eric P. Skaar, Ph.D.

ACKNOWLEDGMENTS

I would like to thank the funding sources that provided the equipment and supplies necessary for this project. The generous support from the Walter Reed Army Institute of Research Grant (W81XWH-17-2-0003) allowed for the completion of this project.

I would also like to thank the members of the Skaar Lab for letting me work in their lab and for teaching me the fundamentals of microbiology research. Additionally, I would like to thank everyone in the Vanderbilt Biophotonics Center for all the support and discussion. Specifically, I want to thank Logan Jenkin for helping me get started on this project and Jeremy Ford for all the help with the Monte Carlo simulations.

TABLE OF CONTENTS

TABLE OF CONTENTS

LIST OF TABLES

Table Page

LIST OF FIGURES

Figure Page

CHAPTER 1

INTRODUCTION

Overview of Skin and Soft Tissue Infections

Epidemiology and Etiopathogenesis

Due to it acting as the 'front line' protection of the body, the skin can commonly become damaged and diseased. A disruption in this important barrier allows for a range of pathogens to easily invade and colonize the body, resulting in a host of different diseases. Of these diseases, microbial invasions of the layers of the skin, as well as the soft tissues found underneath, are particularly common with over 3,000 different diseases of the skin identified [1]. Collectively known as skin and soft tissue infections (SSTIs), this class of disease is the most common infection presentation found in patients visiting the emergency room, with an average incidence in the United States of around 24.6 per 1,000 people per year [2]. However, with the wide variety of possible presentations and a majority of SSTIs being resolved within 7-10 days, this figure most likely underestimates how common these infections actually are.

Despite the high prevalence of SSTIs, healthy skin can ward off the majority of microbial pathogens. This is mainly due to the cutaneous defense mechanisms, including mechanical rigidity, low moisture content, relative acidity, and cooler temperatures, creating an unfavorable microbial environment [3]. However, chemical or physical stress can cause disruptions in the normal physiology of the skin allowing for pathogens to colonize and proliferate the skin. Anything that can affect the skin to the point of potentiating infection and influencing the underlying etiology is deemed an SSTI risk factor. Risk factors can be

divided into two main categories of environmental risk factors and patient-related risk factors [2].

Environmental risk factors, also known as etiological risk factors, are events that either increase the likelihood of encountering a pathogen or disrupt the cutaneous skin barrier. This includes injuries that damage the skin, like animal bites, accidents or invasive medical techniques, as well as activities that increase the likelihood of infection by a specific microbe like with IV drug use, hot tub use, and close contact with someone else infected with an SSTI [2, 4]. Patient-related risk factors, on the other hand, are factors that predispose someone to acquire an SSTI or alter the progression and prognosis of the disease. Depending on the spatial extent, patient-related risk factors can be subdivided as either localized or systemic. As the names imply, localized risk factors are those that only affect the skin, or a portion of the skin, while systemic risk factors are those that affect the entire body. Common localized risk factors include poor skin hygiene and pressure sores while common systemic risk factors include diabetes, malnutrition, and cirrhosis [2, 4].

Anatomical Classification

With how diverse skin and soft tissue infections can present, there was a need for an all-encompassing definition of what constitutes either a skin infection or a soft tissue infection. In 2015, the CDC decided that a skin infection must meet at least one of the following criteria: 1) the patient has purulent drainage, pustules, vesicles or boils; or, 2) patients have 2 or more localized symptoms (pain/tenderness, swelling, erythema/heat) while having at least one positive immunological or histological test including a successful culture from a suspected site (and pure if a common commensal organism); a positive non-culture test from tissue or blood; multinucleated giant cells seen in affected tissue; or a positive

antibody titer for an infectious agent. In a similar vein, a soft tissue infection must meet at least one of the following conditions: successful culture from tissue or drainage; presence of purulent drainage at the affected site; or evidence of an infection at a gross anatomical or histological scale [5]. As mentioned before, over 3,000 different diseases fall into one of these two definitions [1]. To break up this unwieldy number into manageable groups, different methods of classification have been proposed. The three most common classification schemes sort SSTIs by their anatomical site of infection, their microbial etiology, and their severity of the infection [6].

One of the simplest methods of categorizing SSTIs is by the anatomical sites that they affect. This can be further broken down into two subcategories: where on the body the infection occurs and at what depth in the skin [2, 4, 6, 7]. Many skin infections occur due to the resident microflora that can be found normally on the skin. Due to differences in moisture and oxygenation levels, distinct compositions of flora can be found at different points on the body. One major dividing line is the waist with a majority of colonizing flora above the waist consisting of Gram-positive bacteria while the composition below is more of a mixture of Gram-positive and Gram-negative species. This change when moving below the waistline is believed to be due to the proximity to the anorectal region allowing for many enteric species to colonize this region of the skin [4]. Along with this high-level pattern, there are secondary patterns of distribution based on different ideal microbial niches. Due to their higher levels of moisture, the groin, armpit and other intertriginous areas (fat folds, between digits, etc.) tend to have larger populations of microbial flora that contain higher percentages of aerobic species than the average [4]. Further niche patterns also exist including how fungal infections cluster at sites containing nonviable keratinized structures like hair and nails [8]. Understanding this distribution can be of critical importance at the initial stages of diagnosis

as a majority of SSTIs are opportunistic infections caused by flora resident on the skin [9].

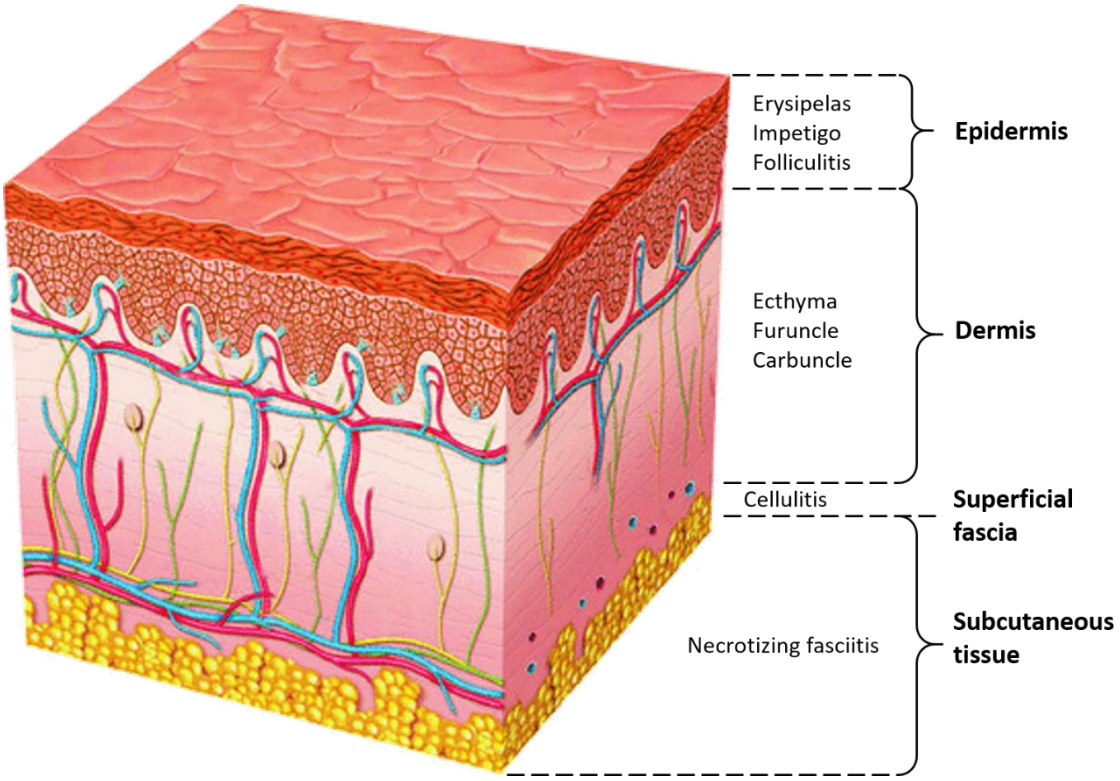

Figure 1.1: Layers of the skin and its common infections. The skin is roughly divided into the protective epidermis and the supportive dermis which are affected by the majority of SSTIs. Below the skin is a layer of adipose tissue and a layer of muscle [14, (modified)].

In comparison to the gross anatomical location, the subcategory of SSTIs based on the depth within the skin that the infection takes place can provide not only information helpful in a differential diagnosis but also typically correlates with the severity of the disease [2, 10]. As can be seen in Fig. 1.1, the skin consists of two major layers, the epidermis and the dermis, which lies on top of a layer of fatty subcutaneous tissue and vestigial muscle [11]. The epidermis is a highly stratified tissue layer typically around 50-100 μm that plays the primary role in protective functions from microorganisms and other harmful substances [12–14]. The epidermis can be broken down into two main strata, the living epidermis and the stratum corneum. The stratum corneum is the outermost layer of the epidermis and consists of terminally-differentiated, squamous corneocytes which have lost all cytoplasmic

organelles, including their nuclei, using that space to form a cornified envelope consisting of cross-linked proteins [11, 12]. It is these envelopes, along with a secreted lipid matrix and strong cell-cell adhesions, that form the permeability barrier that controls water movement and prevents invasion from microbial pathogens [12]. Beneath the ‘dead’ stratum corneum lies the living epidermis consisting of 4 distinct cell layers of differentiating keratinocytes. These layers provide structural support for the stratum corneum, a continuous source of corneocytes for its renewal, as well as microbial protection through the release of various antimicrobial peptides, which form the first line defense against invasion [11, 12].

Supporting the epidermis is the 0.5 to 5 mm thick layer of connective tissue known as the dermis. The strong tensile strength and elasticity of the skin are due to its extensive extracellular matrix made up primarily of collagen and elastin [13]. Along with support, the dermis is home to the blood supply of the skin as no blood vessels pass through the dermal-epidermal junction. The dermal blood vessels are organized into two primary plexus that serve as borders between the papillary, or upper, dermis and the reticular, or lower, dermis [11, 13]. The cutaneous plexus is formed by a network of blood vessels running along the border between the subcutaneous tissue and the reticular dermis. From this network, branches extend to the different cutaneous structures that exist in the reticular dermis including hair follicles, sweat glands and sebaceous glands [13]. Additionally, arterioles spread from the cutaneous plexus to right below the papillary dermis, forming the subpapillary plexus. The papillary dermis is characterized by a pattern of papillae that extend slightly into the epidermis and it is in these extensions that capillary loops form from the subpapillary plexus to supply nutrients and oxygen to the epidermis [13].

Understanding the divisions of the skin can be critically important as different SSTIs tend to be localized to one or more specific locations in the skin and sub-dermal tissues, a

fact that can be utilized for both better differential diagnoses and more targeted treatment strategies [2, 15]. Depending on the depth of the infected layers, an SSTI can either be classified as a superficial infection, in which only the epidermis and/or the papillary dermis is involved, or as a deep infection, where involvement can stretch from the reticular dermis down into the subcutaneous adipose tissue, fascia and muscle [2]. A majority of common skin and soft tissue infections are superficial with notable examples including impetigo, acne, ecthyma, and folliculitis [2, 10]. Impetigo is a superficial infection, being limited to the epidermis, that is particularly common in children. It is characterized by reddening of the skin and the formation of golden crusts [10, 16, 17]. If a case of impetigo progresses down into the papillary dermis, ulcers begin to form beneath the crusts and the infection is upgraded to ecthyma [3]. Acne vulgaris, or common acne, is a frequently caused by infection of the sebaceous glands which are found next to hair follicles in the papillary dermis [2, 6, 9, 18]. Located in a similar location to acne is folliculitis. Folliculitis is an infection or inflammation of the upper portion of the hair follicle, which fully extends down into the reticular dermis [3, 19]. If folliculitis is allowed to progress without being cleared or treated, it can progress to various deep SSTIs discussed below.

While not as common as superficial infections, deep SSTIs tend to require more attention and care. The most common deep infections are furuncles and carbuncles, cellulitis and necrotizing fasciitis [2, 10]. When a case of superficial folliculitis fully invades down into the hair follicle, a furuncle, or boil, forms resulting in a tender red nodule that can exude pus [3, 19]. If neglected or mistreated, furuncles can laterally extend resulting in the coalescence of multiple furuncles to form a deeply interconnected abscess known as a carbuncle [3, 19]. When an infection takes place outside the hair follicle in either the reticular dermis or subcutaneous tissue, it is most likely cellulitis. Cellulitis typically presents as a

diffuse infection characterized by a rapidly spreading area of pain and erythema with indistinct borders. Due to the proximity to the dermal lymphatics and the cutaneous plexus, progression to lymphangitis or septicemia are common [3, 17]. One of the most destructive and life-threatening SSTIs is necrotizing fasciitis or 'flesh-eating' infection. Located in the subcutaneous tissue and fascia, necrotizing fasciitis initially presents as erythema, pain, and edema before progressing to dark violet plaques that necrose within 48 hours [3, 17, 19]. If suspected, immediate chemical and surgical interventions are required.

Severity Classification

Due to deep infections localizing near more critical tissues and having greater access to the blood supply than superficial, there is a clear trend of superficial SSTIs being milder with less complicating factors and deep infections usually require greater attention and care. As the outward presentation of an SSTI can be similar between disparate infections, it would be ideal to be able to directly probe the depth of involvement during an examination, thus improving the diagnosis and elucidating the urgency of treatment [20]. Unfortunately, such a direct measure is currently infeasible in a clinical setting [15].

With this in mind, the most common classification scheme used in the clinic organizes SSTIs based on their perceived severity [20]. To assess the severity of an unknown infection, the presence or absence of various complicating factors are determined and the SSTI is deemed as either a complicated or uncomplicated SSTI [2]. This classification scheme is advantageous as while many superficial infections are innately uncomplicated, immunosuppressing factors, such as diabetes and HIV-infection, can cause what would normally be a mild, superficial infection to progress into complicated infection requiring more thorough attention [5, 7]. Additionally, SSTIs that would normally be classified as

uncomplicated can be automatically upgraded to complicated when they occur in specific anatomical locations like rectal abscesses, or involve anaerobic or Gram-negative organisms [2]. This flexibility allows for this method of classification to best inform first-line decisions and actions.

Thinking that this binary approach to severity limits the usefulness of this type of classification, some groups have attempted to create more nuanced classifications schemes. Once such approach by the Infectious Disease Society of America has broken SSTIs down into three categories: superficial and uncomplicated infections; necrotizing infections, bite and animal associated infections, and surgical site infections; and infections in immunocompromised hosts [6, 21]. While not purely based on severity criteria, these groups effectively span the range of all possible severities and can help determine the level of treatment required. Another approach outlined by Eron *et al*. defined four classes of infections based on the local and systemic symptoms with the goal of creating a system that could guide the clinical management of an unknown SSTI. Class 1 infections are those in which the patients have no signs of systemic toxicity or co-morbidities; class 2 infections are associated with patients who are either stable with systemic symptoms or are systemically well but have some form of co-morbidity than can complicate the resolution of the infection; class 3 infections produce strong systemic toxins or symptoms, like fever, tachycardia, and hypotension; class 4 infections have gone septic and are life-threatening like necrotizing fasciitis [6, 20]. While this method does not broadly distribute SSTIs among the different classes, placing a majority into class 1, such a specific focus on the most severe of infections can help a clinician to determine if immediate hospitalization or surgery is required.

Etiological Classification

The most definitive categorization of skin and soft tissue infections stems from identifying the underlying infectious agent. There are three main categories of microbial infectious agents and while they might vary in their prevalence in the skin, bacteria, fungi, and viruses can and do cause infections in the skin [2, 5, 6, 16, 17]. While protozoans and arthropods are known to be able to cause skin infections, they are not discussed here due to their rarity [6].

Viral infections that involve the skin come in two types: infections in the skin itself and infections elsewhere that cause symptoms to appear in the skin. While the pool of viral SSTIs is way too varied to discuss here in depth, there are common and well-known viral infections that fall into both of the previously mentioned categories. For viruses that primarily infect the skin itself, warts are the most prevalent [17, 22]. Various types of warts are all caused by human papillomavirus infecting the epidermis of a localized spot causing the formation of benign skin growths [17, 19]. The infection can commonly be diagnosed due to the relatively unique appearance of its growth, though treatment may be unnecessary as they are commonly self-limiting.

Unlike warts which directly infect skin cells, there are a number of systemic viruses that present with strong skin-based symptoms. The most common of these viral infections are four of the childhood exanthems: measles, rubella, fifths disease, and roseola [22]. While each is caused by a different virus, all four of these diseases present with maculopapular rashes caused by the body's immune response trying to fight off the infection. This class of viral infections can typically be diagnosed from their characteristic wide-spread rash, but verification is required as bacterial and non-infectious, irritating agents can produce similar rashes [17, 22].

Fungal infections typically stratify themselves by the type of environment they require. Dermatophytes require a source of keratin as a food source and are thus typically found in hair and nail beds. This includes common diseases such as athlete's foot (tinea pedis) and ringworm (tinea corporis) which both commonly present with dry, scaly skin at the affected areas, a characteristic common to most fungal infections [8]. Besides dermatophytes, the most common fungal pathogen of the skin is the yeast *Candida albicans*. Typically occurring in moist, occluded sites, cutaneous candidiasis does not present like other fungal skin infections, instead causing rash, erythema, and severe itching. It can also present at pustules that can be easily mistaken for bacterial folliculitis [8].

While the skin acts in balance with a suite of bacterial flora to maintain normal health, these same bacteria can become opportunistic pathogens if that balance is broken [9]. Due to different ideal environments for different bacterial species, bacterial flora populations are highly varied between different topographical sites and microenvironments; despite this, a majority fall into three main phyla: Actinobacteria, Proteobacteria, and Firmicutes [18]. When the most common members of these phyla are examined, an interesting trend appears: all three contain species that commonly cause human skin infections. Firmicutes has methicillin-resistant *Staphylococcus epidermidis*, a common cause of wound infections, Actinobacteria has *Propionibacterium acnes* which is commonly associated with the lesions of acne vulgaris, and Proteobacteria has *Enterobacteriaceae* spp. which cause chronic ulcers [2, 4]. On top of the resident flora, human skin is visited by a wide variety of transient flora that require a breakdown in the epidermal barrier to allow for colonization [2, 3]. Due to the trend of these species having strong virulence factors to help them establish an infection, transient flora are the underlying agents of a majority of SSTIs that require hospitalization [6]. The most common transient flora that cause skin infections include *Staphylococcus aureus*, which can

range in severity from impetigo to cellulitis and abscesses, and *Pseudomonas aeruginosa*, a common cause of chronic wounds and hot-tub folliculitis [7, 23]. While bacterial skin and soft tissue infections as a whole are broad and complex, this work focuses on Gram-positive bacteria and further detail into infections caused by Gram-positive bacteria will be explored below.

Gram-Positive Bacterial Skin and Soft Tissue Infections

When discussing bacterial infections of any kind, one of the primary forms of categorization is to divide the infectious bacteria into two fundamental varieties of cells encompassed by the Gram-positive/Gram-negative distinction [2, 4, 5, 7, 9, 16, 19, 20]. Strictly speaking, this distinction stems from the differential results of a Gram stain in which bacterial cells are dyed with crystal violet dye. Gram-positive bacteria retain the dye after being washed in alcohol while Gram-negative bacteria do not [24]. While this seems like an innocuous difference, the differential staining response is due to an array of chemical and structural differences between the two bacterial varieties. One of the main differences between the two, and the actual reason for the variance in Gram-staining, lies in the structure of the cell wall and cell membrane.

While all bacteria have a cell wall outside of their cytoplasm composed of cross-linked peptidoglycan, Gram-positive bacteria have a thick layer of peptidoglycan surrounding their outer membrane while Gram-negative bacteria have a much thinner layer that is situated in their periplasm, the space between their inner and outer membranes [24–26]. It is due to this difference in thickness that the crystal violet dye can be washed from Gram-negative bacteria. Other key differences between Gram-positive and Gram-negative bacteria include different mechanisms of secretion, which allow for diverse

mechanisms of antibiotic resistance, and differences in key metabolic pathways, like the production of heme which will be discussed in further detail below [25, 27–30].

Categorizing bacterial pathogens into these two cell varieties is important as Gram-positive bacteria tend to play the greatest role in patients hospitalized with an SSTI, with only 15% of cases having a positive culture of a Gram-negative bacteria of any kind [5]. Early clinical identification is important as it allows for more targeted, effective therapies to be used [5, 16, 20]. This lopsidedness in the prevalence of Gram-positive pathogens is primarily due to the overwhelmingly high prevalence of *Staphylococcus aureus* in skin infections. *S. aureus* is such a dominant pathogen in the skin that in 2003 it was identified as the causative agent in over 40% of all SSTIs [2, 5, 6, 20, 21, 31]. Part of the reason behind this prevalence is the ability of *S. aureus* to cause a variety of different types of skin infections ranging broadly in localization and severity. It is commonly found to cause uncomplicated, superficial infections like impetigo and folliculitis, but also is a common cause of deep, complicated infections like cellulitis, furuncles, carbuncles and wound infections [2, 16, 21].

Despite the overwhelming pervasiveness of *S. aureus* bolstering the numbers, other Gram-positive bacteria frequently infect the skin. The next most common set of Gram-positive pathogens include various *Enterococcus* species like *E. faecalis*, which is prevalent in cellulitis and chronic ulcers below the waist due to its presence in the 'fecal veneer' [2, 4, 5, 32]. β-hemolytic *Streptococci* are another commonly found group with members like *Streptococcus pyogenes* which is a common cause of ecthyma and necrotizing fasciitis in human bite wounds due to it being commonly found in normal throat flora [2, 3, 17]. While it does not cause as severe of infections as compared to the previously mentioned species, *Propionibacterium acnes* is a common Gram-positive member of normal skin flora that can

cause acne vulgaris, the most common skin condition treated by doctors [1, 2, 9, 18].

The Rise of Antibiotic Resistance

Surprisingly, there is a large debate over how valuable microbial cultures and analysis are when treating skin or soft tissue infections. The main opposition to running these tests is that bacterial infections are such a dominant percentage of the infections, it is easier to immediately treat with broad-spectrum antibiotics and only pursue further diagnostic tests when the infection shows no signs of improving [6]. However, over-prescription of antibiotics, especially broad-spectrum antibiotics, has been documented to induce an increase in the percentage of the bacterial population that are drug resistant [33–35]. For example, using long-term antibiotic treatment to reduce acne lesions has been shown to be directly connected to the acquisition of antibiotic resistance [18].

While development of resistance to antibiotics has been well documented since the early days of antibiotic use, the rate at which new drugs were being discovered was sufficient enough to overcome any new resistances that were developing. However, in recent years, the rate at which new antimicrobials have been discovered and approved for human use has dwindled while the prevalence of resistance has continued to climb [33, 34, 36]. This has led to the recent development of multi-drug resistant strains that have acquired resistance towards more than one common antibiotic as well as strains that have developed resistance to what used to be our ‘last resort’ drugs like vancomycin-resistant enterococci [5, 34, 37].

Possibly the most infamous case of antibiotic-resistant bacteria is *Staphylococcus aureus*, primarily due to its high prevalence. As mentioned previously, SSTIs caused by *S. aureus* can range drastically in severity from self-resolving to life-threatening [2, 16, 21]. One of the major reasons for this diversity in the presentation is that many *S. aureus* strains

have begun carrying genes that provide resistance to a variety of different antibiotics [38, 39]. Out of all forms of resistant *S. aureus*, methicillin-resistant *Staphylococcus aureus*, or MRSA, is by far the most common, both in prevalence and in public awareness. While this name may imply resistance to just a single antibiotic, it actually represents resistance to all β-lactam-based antibiotics including penicillins, carbapenems, monobactams, and cephalosporins [40]. While there have been improvements in recent years in combating MRSA, it is still a major problem, causing 19,000 deaths and 360,000 hospitalizations in the United States each year [39]. The prevalence of MRSA has become so ubiquitous that some countries report 50% or more of clinically isolated *S. aureus* strains are a form of MRSA [6, 37].

While other classes of antibiotics can still be used to combat MRSA infections, there is a rising risk of fostering further resistance and developing pathogens resistant to multiple classes of drugs. The current drug of choice for treating SSTIs when MRSA involvement is suspected is the cell wall biosynthesis inhibitor vancomycin [21]. While highly effective at eliminating MRSA, clinical isolates of *S. aureus* with reduced susceptibility, or complete resistance, to vancomycin therapy have emerged in the past 20 years [41]. To address this and stop antibiotic resistance from progressing further, the development of novel drugs and therapies that minimize or eliminate the potential of resistance is critical.

Antimicrobial Photodynamic Therapy

Overview

One potential treatment method that has shown promise for treating skin and soft tissue infections with minimal development of resistance is antimicrobial photodynamic therapy

(aPDT) [42]. Originally developed as a cancer therapy, photodynamic therapy has expanded into a technique to treat various skin disorders, dental carries and microbial infections [43–45]. At its core, PDT is a two-step technique where, first, a non-toxic molecule known as a photosensitizer (PS) is either administered to or induced in the tissue of pathogen of interest. After allowing for a period of incubation the area is illuminated with a specific wavelength of light to activate the photosensitizers leading to the generation of cytotoxic reactive oxygen species (ROS) when in the presence of oxygen [46–48]. As their name implies, reactive oxygen species are a group of oxygen-containing molecules that easily react with and oxidize key biomolecules like proteins, DNA and lipids [42, 49]. When at a sufficient concentration, these oxidation events accumulate eventually leading to cell death.

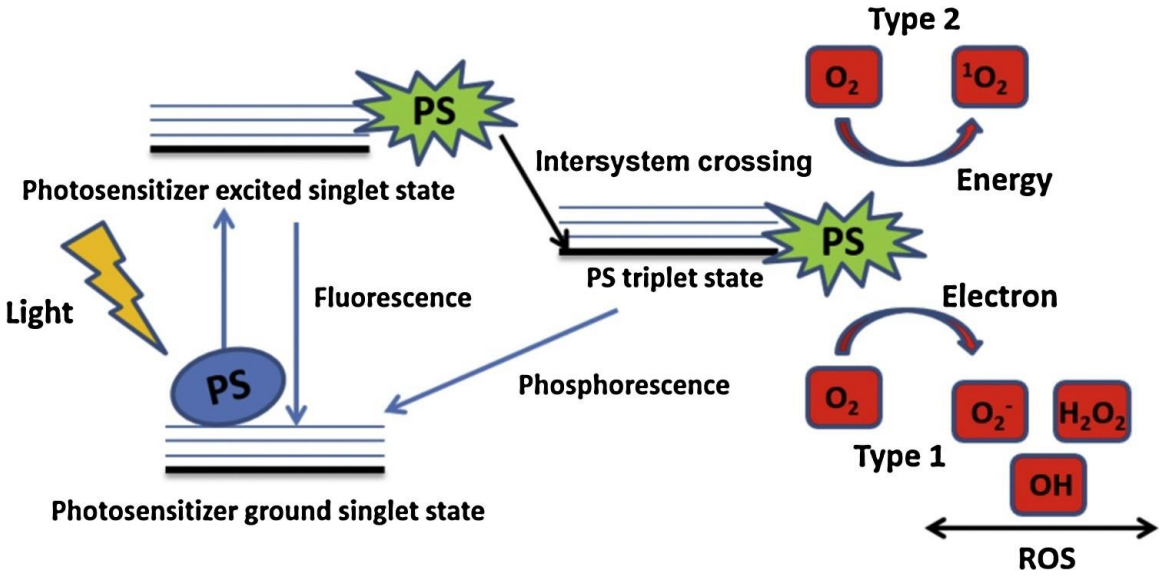

Figure 1.2: Jablonksi diagram of PDT mechanisms. Photosensitizers absorb light to promote an electron to the singlet excited state form which it can undergo intersystem crossing to form a long-lived excited triplet state. From this state, photosensitizers can transfer an electron (Type 1) or energy (Type 2) to molecular oxygen resulting in oxygen radicals and singlet oxygen, respectively [42].

Out of the entire process of PDT, the most important steps are the absorption of light by the photosensitizer and the transfer of that absorbed energy to another molecule (Fig. 1.2). After incubation, the accumulated photosensitizers are in a singlet, ground state having a pair of electrons with opposite spins in a low energy molecular orbital. A PS molecule is capable

of absorbing wavelengths of light whose corresponding energy matches the energy difference between the ground state and the first excited state of the PS. After absorption of such a photon, one of the two electrons in the pair is promoted into the higher energy orbital while maintaining its spin, allowing the PS to exist in a singlet excited state [42, 46, 48, 50]. This state is extremely short-lived with a half-life of only 10^{-10}-10^{-7} seconds [51].

While the PS must return to the ground state, there are multiple avenues that the released energy can take. Most commonly, the PS can undergo internal conversion and release the excess energy as heat. Additionally, most PSs are capable of fluorescence, releasing the absorbed energy as a lower energy, longer wavelength photon [51]. More importantly, however, is that PS molecules can undergo a process known as intersystem crossing in which the spin of the excited electron reverses to form a parallel electron pair, transitioning the molecule from its singlet excited state to a triplet excited state. Similar to the singlet state, the excited triplet electron can return to the singlet ground state by emitting a lower energy photon though phosphorescence [46, 48, 51]. However, as moving between triplet and singlet states requires a change in electron spin, violating the spin selection rule, it is known as a forbidden transition and thus has a low probability of occurring. This effectively 'traps' the electron in the triplet state for 10^{-6}-10 seconds, delaying its return to ground state [51]. It is from this triplet excited state that photosensitizers can react with molecular oxygen to produce various cytotoxic reactive oxygen species [42, 46, 48, 50].

When in the excited triplet state, there are two primary photochemical reactions, each resulting in different cytotoxic species. Type I reactions occur when the triplet state PS undergoes an electron transfer reaction, forming a PS radical ion, before reacting with molecular oxygen to produce the radical anion superoxide ($O_2^{\bullet -}$). While cytotoxic itself, reduction of dismutation of superoxide yields cytotoxic hydrogen peroxide (H_2O_2) which

can be further reduced to give hydroxy radicals ($HO^{\bullet}$), a powerful oxidant. In contrast, Type II reactions generate ROS in a much more simplistic manner. Instead of undergoing any form of election transition, the long triple state lifetime allows for the PS to collide with molecular oxygen, a relatively unique molecule in that it exists in a triplet ground state. This allows for the excited triplet PS to directly transfer its energy to molecular oxygen leading to the formation of singlet oxygen ($^1O_2$) and a return of the PS to its ground state [42, 44–50]. While all photosensitizers are theoretically capable of producing ROS through both Type I and II mechanisms, the relative abundance of each method varies between classes of PSs and the local environment [50]. However, it is believed that most clinically applied PSs act primarily by producing singlet oxygen through the Type I photochemical process [46].

Methods of Antimicrobial Photodynamic Therapy

When reactive oxygen species are generated at a sufficient concentration, they will induce cell death indiscriminately. As bacterial infections necessarily involve having pathogenic microbes in close proximity to host tissue, indiscriminate ROS production can lead to unwanted collateral damage. However, singlet oxygen has a very short lifetime of 10^{-9}-10^{-6} seconds which limits its diffusion to only 10-55 nm [46, 48]. Thus, singlet oxygen is limited to oxidizing only nearby biomolecules and is unlikely to cause damage far from where it was generated. As an ideal therapy involves eliminating the pathogen while minimizing or eliminating collateral damage, successful aPDT must ensure that the majority of generated ROS is localized in or around the bacteria. The most efficient way to control the localization of singlet oxygen is by utilizing photosensitizers that preferentially accumulate to the desired cell types. When targeting bacteria, there are three different mechanisms in which this is accomplished, two using exogenously supplied photosensitizers

and one using photosensitizers produced endogenously by the bacteria.

The most commonly used exogenous PSs for aPDT all utilize the same mechanism for localization. This broad group contains a wide variety of different classes of PSs including phenothiazinium chromophores, like the classical PSs methylene blue and toluidine blue, porphyrin and phthalocyanine derivatives, like TMPyP, and modified fullerenes. Despite this wide variety of molecular structures, members of this group share one common characteristic: the presence of at least one positive charge [52]. This positive charge allows for an electrostatic interaction between the cationic PS and the bacterial cell walls that have an overall negative charge due to teichoic acid in Gram-positive bacteria and lipopolysaccharides in Gram-negative bacteria [53]. It has been shown that by simply modifying the PSs in this class to contain more positive charges, the specificity and efficacy of treatment rise significantly [48, 52]. As cation-based photosensitizers cannot guarantee complete specificity to bacteria and are unable to target specific bacterial species, some groups have employed photosensitizers that have been conjugated to monoclonal antibodies [48, 52]. While care has to be taken to ensure that the functionality of both the antibody and the PS are not impaired by the conjugation, successful conjugation has shown efficacy in treating a number of different infections in mouse models [54, 55]. The main drawbacks to this method, however, are its inability to treat infections caused by a mixture of different bacterial species and its failure in acting as a topical treatment due to the large size of the conjugated molecule limiting how far it can diffuse into the skin [20, 52].

Instead of supplying an exogenous molecule, a common method of photosensitizing cells is to induce the accumulation of endogenous molecules that act as photosensitizers. Almost exclusively, this is achieved by perturbating the heme biosynthesis pathway resulting in the accumulation of protoporphyrin IX (PPIX), a method that will be explored in further

detail below [30, 46–48, 50, 56].

Endogenous Porphyrin Photosensitization

Endogenous porphyrins are a life-sustaining class of molecules that are closely tied to the metabolism of living organisms. In general, they are macrocyclic molecules, containing four pyrrole rings that are linked together via methine bridges. This conformation allows for the porphyrin nucleus to have a space that allows it to act as a tetradentate ligand, using four donor atoms to complex with metals, with transition metal ions granting the greatest overall stability to the molecule [57]. It is this ability to complex with metal atoms that grants porphyrins their most useful roles, with iron-complexed porphyrins in hemoproteins, magnesium-complexed porphyrins in chlorophylls, and cobalt-complexed in Vitamin B12 [57]. On top of these necessary functions, porphyrins also act as efficient photosensitizers that have been utilized exogenously and endogenously to treat cancer, age-related macular degeneration, skin disorders, and infections [30, 46–48, 50, 56, 58].

The cofactor heme, consisting of a porphyrin ring complexed with iron, is essential for many for many different forms of life. Heme is required for cellular respiration, serving as an electron shuttle in the electron transport chain. Additionally, it acts as a redox-active moiety that is required for the activation and function of critical proteins including hemoglobin and catalase. Due to how ubiquitous the need for heme is, almost every organism has a method of biosynthesizing heme [29]. With animals using glycine and succinyl CoA, and plants, bacteria and archaea using glutamate-1-semialdehyde derived from glutamyl-$tRNA^{Glu}$, the heme-precursor δ-aminolevulinic acid (ALA) is produced in a rate-limiting manner (Fig. 1.3) [29, 59, 60]. Thus, when cells are provided with excess exogenous ALA, this rate-limiting step is bypassed, and downstream intermediates accumulate.

This process is important as it is what allows for the application of ALA to cause the accumulation of PPIX, resulting in photosensitization of heme producing cells. While this process is inherently non-specific due to ALA serving as a universal heme precursor, the variability in metabolic rate and iron availability allows for different cell types to react with different sensitivities to ALA. As pathogenic bacteria are usually iron starved, due to the sequestering of iron by the host, and they have elevated baseline porphyrin levels as compared to the surrounding tissue, they tend to have a slightly higher sensitivity to ALA. Despite this, topical ALA application still produces the unwanted side-effect of diffuse photosensitization of the skin which has led to its use in antimicrobial photodynamic therapy being reduced over the years.

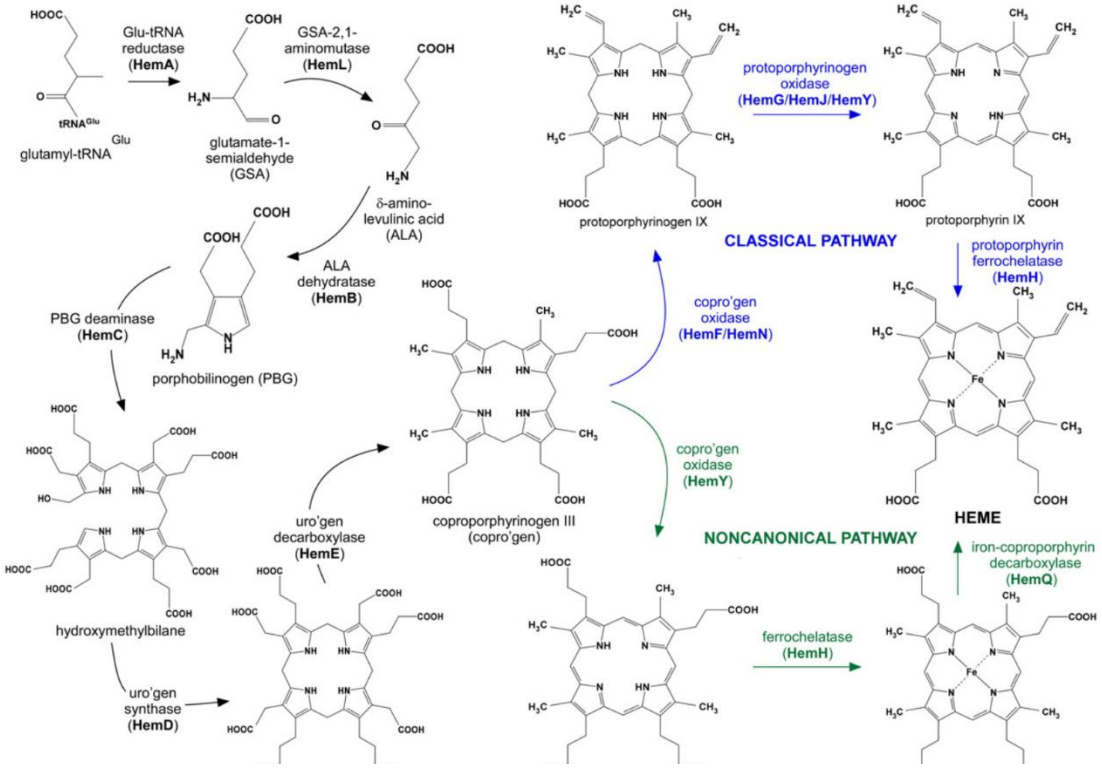

Figure 1.3: Bacterial heme biosynthesis. Bacteria, and other heme producing organisms, begin heme biosynthesis with the production of the universal precursor ALA. After several conserved enzymatic steps, ALA is converted into the coproporphyrinogen III. In the classical pathway (blue), Gram-negative bacteria and eukaryotes produce heme using the intermediate protoporphyrin IX. Gram-positive bacteria utilize a noncanonical pathway (green) in which heme is produced using coproporphyrin III as an intermediate [29].

However, it was recently discovered by Dailey *et al*. that the process of heme biosynthesis is not as conserved as was once hypothesized [28]. They found that Gram-positive bacteria deviate from the classical heme biosynthesis pathway after coproporphyrinogen III (CPGIII), utilizing coproporphyrin III as an intermediate instead of PPIX (Fig. 1.3) [28, 60]. While this difference does not have an immediate effect on the usefulness of utilizing heme production to photosensitize gram-positive bacteria, due to ALA application still resulting in porphyrin accumulation, it has opened up the opportunity to target the Gram-positive specific enzymes to induce specific photosensitization. One such method targets the Gram-positive enzyme coproporphyrinogen oxidase (CgoX, formerly HemY). CgoX is the first unique enzyme in the noncanonical pathway, converting CPGIII into CPIII through a six-electron oxidation event [28, 29, 60]. Surdel *et al*. identified that the

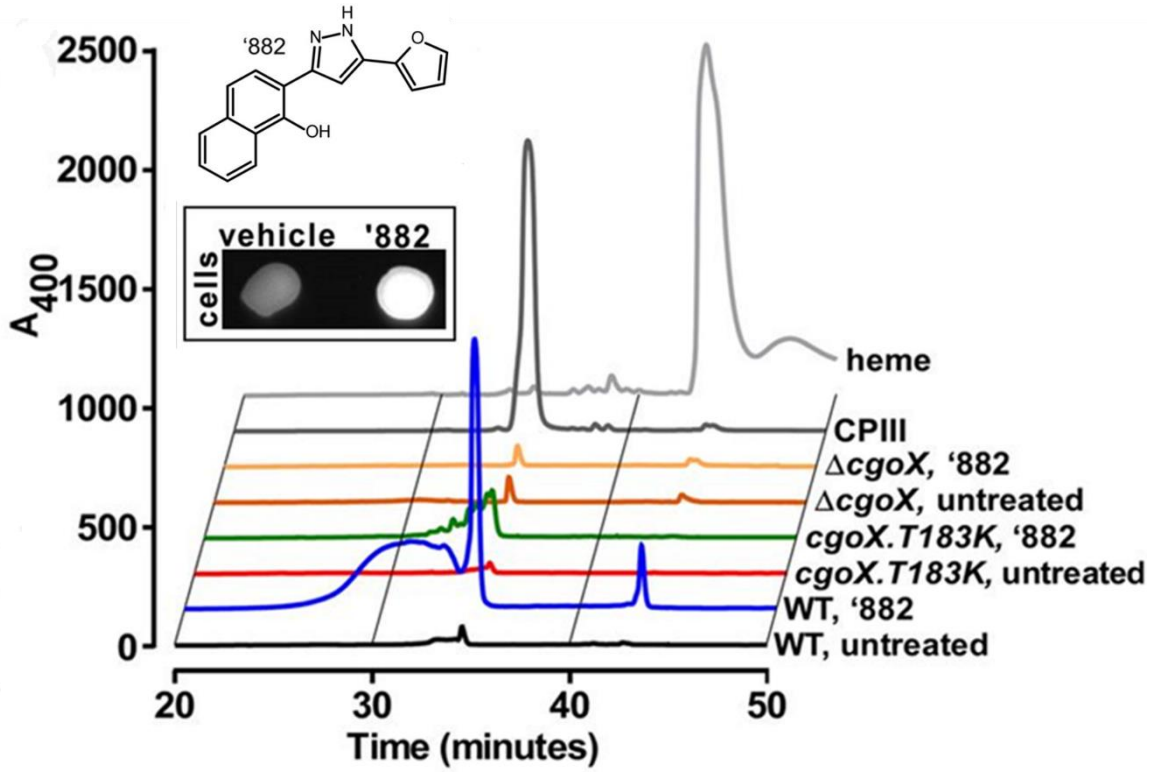

Figure 1.4: '882 exposure increases CPIII production. The application of the small molecule '882 induces accumulation of CPIII in *S. aureus* leading to fluoresence (inset). HPLC analylsis using the absorbance at 400 nm of WT and CgoX deficient mutants reveals that '882-induced CPIII accumulation is dependent on CgoX function [30, (modified)].

small molecule VU0038882 (‘882), which was known to activate the heme-sensing two-component system of *S. aureus*, serves as an activator of CgoX, leading to CPIII-mediated photosensitization of a variety of different Gram-positive species including *S. aureus* (Fig. 1.4) [30, 61]. This new method of endogenous photosensitization is ideal since, due to it targeting a Gram-positive specific enzyme, ‘882 is capable of photosensitizing bacteria without the risk of doing the same to the surrounding tissue. Additionally, as ‘882 uses a new method to induce CPIII accumulation, it is capable of acting synergistically with ALA to produce a greater extent of photosensitization [30].

All porphyrins, due to their similar core structure, have a characteristic absorption spectrum of ultra-violet and visible light. The spectrum consists of a sharp, main absorption peak near 400 nm, known as the Soret band, followed by four weaker absorption peaks between 450 and 700 nm, known as the Q-bands (Fig. 1.5) [62, 63]. While the pattern is similar, differences in the side chains attached to the main aromatic ring alter the location and strength of both the Soret band and the Q-bands. As previous attempts of ALA-aPDT have operated under the assumption that the underlying photosensitizer in Gram-positive

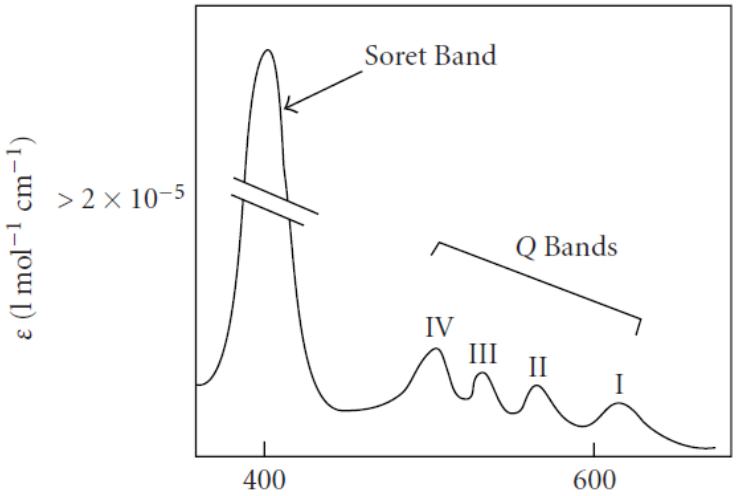

Figure 1.5: Porphyrin absorption spectrum. Porphyrins have a primary absorption peak near 400 nm called the Soret band as well as four minor absorption peaks between 450 and 700 nm called the Q-bands [62].

bacteria is PPIX, they did not achieve optimal activation of CPIII [64–66]. To address this, chapter 2 will explore the optimal application of light to drive CPIII-mediated aPDT.

Depth of Light Penetration

The ideal light source for any PDT application has a wavelength that is both highly absorbed by the target PS and minimally absorbed by the surrounding tissue. For PDT using porphyrin as the primary PS, the ideal wavelength is approximately 400 nm, targeting the Soret band. Unfortunately, as seen in Fig. 2.7a, blue light, around 400 nm in wavelength, is highly absorbed by the skin. This results in a rapid attenuation of blue light as it travels into the deeper layers of the skin. This effect is so strong that 400 nm light can only travel around 160 μm into the skin, barely reaching the papillary dermis, before its intensity falls to $1/e$ (or 37%) of its original value. As bacterial SSTIs are commonly localized in the papillary dermis, reticular dermis and subcutaneous fascia, using blue light to drive aPDT is limited except in treating superficial infections. In chapter 2, we will address the effectiveness of using Q-band targeted light in CPIII-aPDT and compare its predicted effectiveness in depth with blue light PDT.

CHAPTER 2

PHOTODYNAMIC THERAPY OF *STAPHYLOCOCCUS AUREUS* USING ENDOGENOUS COPROPORPHYRIN III

Introduction

Due to its constant interaction with the environment, the skin is continuously colonized by a host of microbial life. When the protective functions of the skin become compromised, these microbes are able to invade and infect the skin as well as the underlying adipose tissue and muscle. Known as skin and soft tissues infections (SSTIs), this class of infections is extremely common with around 2.5% of people in the US each year experiencing one [2]. However, as many of SSTIs resolve themselves without treatment, this is most likely an underestimate of the incidence rate.

Despite being caused by all forms of microbial pathogens, the vast majority of SSTIs tend to be caused by some form of bacterial agent. Most commonly, these infections are cause by Gram-positive bacteria with only 15% of all positive SSTI cultures containing a Gram-negative pathogen [5]. This wide disparity in prevalence is mostly due to dominance of *Staphylococcus aureus* in SSTIs. While normal *S. aureus* infections can be serious in their own right, the risk and burden of treating these infections has been compounded with the increasing rise of antibiotic-resistant bacteria with methicillin-resistant *S. aureus* (MRSA) being especially common. MRSA has become so common in the US that some hospitals report MRSA incidence rates that are on par with those of methicillin-susceptible *S. aureus* [67]. While non-penicillin-based antibiotics can still currently treat MRSA infections, continued use of antibiotics increases the risk of fostering new multi-drug resistant strains. To prevent this, novel drugs and treatments that minimize or eliminate the potential for the

development of resistance are required.

One potential method that has shown promise in this regard is antimicrobial photodynamic therapy (aPDT). Originally developed as method to treat cancer, PDT works by administering or inducing the accumulation of a non-toxic molecule known as a photosensitizer (PS). After allowing for incubation the area is illuminated with light of a specific wavelength in order to activate the photosensitizers which leads to the generation of cytotoxic reactive oxygen species (ROS), namely singlet oxygen. The produced ROS then induces cell death after oxidizing multiple key biomolecules like proteins, DNA and lipids [42, 49]. As the mechanisms of action of ROS are nonspecific and bacterial infections necessarily involve having the bacteria in close proximity to skin cells, indiscriminate ROS production can lead to unwanted damage of the skin or other tissues. However, the lifetime of singlet oxygen is short enough that it can only oxidize molecules in its immediate surroundings [46, 48]. This means that if you can control the localization of PS to only the bacteria, collateral damage can be prevented.

The method of inducing an accumulation of endogenous photosensitizer in a cell takes advantage of the heme biosynthesis pathway. By supplying excess δ-aminolevulinic acid (ALA), a rate-limited precursor, the pathway continues to run resulting in an accumulation of protoporphyrin IX (PPIX) [29, 59]. However, as this process is nonspecific, affecting both host cells and bacteria, its use has fallen out of favor in recent years. However, it has recently been discovered that Gram-positive bacteria deviate away from the canonical method of heme production, utilizing coproporphyrin III (CPIII) instead of PPIX [28, 60]. This difference has opened up Gram-positive bacteria to being specifically photosensitized by directly upregulating the enzymatic activity of CgoX, the bacterial enzyme that produces CPIII [30]. As previous attempt of endogenously photosensitizing Gram-positive bacteria

have operated under the prior assumption that the target photosensitizer is PPIX, the chosen light sources were not optimally activating CPIII [65, 66]. Thus, it is unknown how effective CPIII is as a photosensitizer.

The purpose of this study was to determine the efficacy of killing Gram-positive bacteria using coproporphyrin III-mediated antimicrobial photodynamic therapy (CPIII-aPDT) and to gauge the feasibility of using this technique to treat skin and soft tissue infections. I tested the hypothesis that the previous reports of poor efficacy were due to targeting the wrong photosensitizer. Additionally, the effectiveness of utilizing secondary absorption peaks to activate CPIII-PDT was explored. After creating a model to predict the effectiveness of using different wavelengths of light to target different depths in the skin, the effects of using more than one light source of different wavelengths were explored.

Materials and Methods

Bacterial Strains and Growth Conditions

The representative Gram-positive bacteria used in this work was the USA300 LAC strain of *Staphylococcus aureus*, a community-acquired methicillin-resistant *S. aureus* strain. Cells were aerobically cultured on tryptic soy agar (TSA) at 37°C for 24 hours. Overnight cultures were made by collecting and inoculating single colonies in 3 mL tryptic soy broth (TSB) before growing under dark, aerobic conditions in a shaking incubator (New Brunswick Innova 44; Eppendorf) at 180 rpm and 37°C for 18 hours.

Porphyrin Absorbance Measurement

To confirm the absorption characteristics of coproporphyrin III (Frontier Biosciences) and protoporphyrin IX (Sigma-Aldrich), absorbance measurements were taken

of each. Using a 100 μM solution of the chosen porphyrin in DMSA, an absorbance spectrum was measured using a Varian Cary 50 Bio UV-Vis Spectrophotometer (Agilent Technologies). Measurements of three different samples were taken and averaged to obtain a spectrum between 300 and 900 nm with a spectral resolution of 0.5 nm and a spectral bandwidth of 1.5 nm (Fig 2.1).

Light Sources

To effectively target different sections of the coproporphyrin III absorption spectrum, five different LED light sources were obtained from ThorLabs and used in this work (Table 2.1). Each LED was powered using a T-cube LED driver (LEDD1B; ThorLabs) that

Table 2.1: LED parameters

Parameters	M395L4	M415L4	M565L3	M617L3	M680L4
Center Wavelength (nm)	395	415	565	625	690
FWHM (nm)	16	14	104	18	22
Viewing Angle (degrees)	126	138	125	80	18
Maximum Current (mA)	500	1500	1000	1000	600
Spot Radius at Sample (cm)	1	1	1	1	1
Irradiance at Sample (mW/cm^2)	32	40	48	45	16

supplied current equal to the respective maximum current limit of the diode. To determine the wavelength sensitivity of targeting the CPIII Soret band, two high-power, blue LEDs with different center wavelengths were used. The 415 nm LED (M415L4) was used to represent light sources used in traditional PPIX-mediated aPDT while the 395 nm LED (M395L4) was used to optimally target the measured maximum absorption of CPIII. To determine the effectiveness of CPIII-mediated aPDT when targeting the Q-bands, three different LEDs were used. The 565 nm LED (M565L3) was utilized as a broadband light source that would target multiple Q-bands simultaneously. In comparison, the 625 nm LED

(M617L3) was used for activation of the fourth Q-band of CPIII, a common method of activation in PPIX-mediated PDT. Lastly, a 690 nm LED (M680L4) was used to determine what effects, if any, occur when attempting to drive CPIII-aPDT outside of the main absorption peaks (Fig. 2.1).

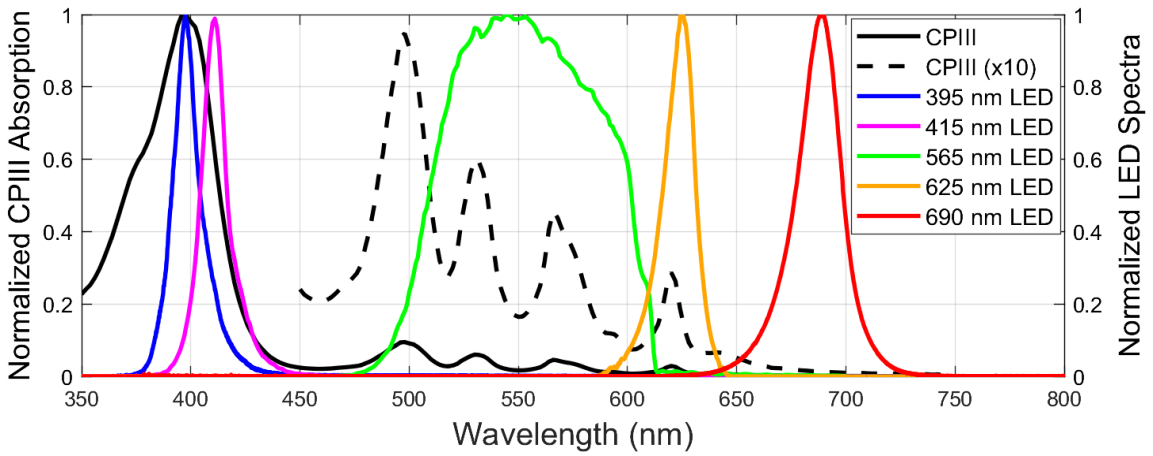

Figure 2.1: Spectra of light sources and CPIII absorption. Light sources were chosen to provide different degrees of activation of CPIII by targeting different absorption bands and to achieve deeper penetration of light.

Optical Setup and Analysis

Two separate optical setups were used to collect and deliver the light emitted by the diodes to sample. The ultimate goals of both setups were to collect the highly divergent light emitted from each of the diodes and allow for different diode outputs to be spatially combined at the sample illumination plane. Both the first and second setup accomplished the second goal by utilizing two long-pass dichroic filters, one with an edge wavelength of 470 nm (FF470-Di0; Semrock Inc.) and another with an edge wavelength of 605 nm (FF605-Di02; Semrock Inc.). This allowed for the outputs of either of the two blue lights, either of the two red lights and the 565 nm light to be combined.

To collect the emitted light and deliver it through the beam splitters with minimal losses, the first setup used a single aspheric condenser lens (f=20 mm, NA=0.6; ACL2520U;

ThorLabs) approximately 1 cm in front of each diode. To account for the differences in pathlength and angular divergence, the distance between each diode and lens was adjusted so that a 1 cm spot size was obtained at the sample. The second optical setup aimed to improve upon the first design by shaping each beam such that it would have an approximate top-hat, or super-gaussian, intensity profile at the sample.

To accomplish this, new collection optics and delivery optics were designed and optimized using Zemax OpticStudio (Fig. 2.2). Replacing the single aspheric condenser lens, two of the condenser lenses where stacked to create an air-filled pseudo-doublet (C_1) approximately 500 μm from the surface of the diode. This configuration collects a majority of highly divergent emitted light and delivers it through the dichroic filters to the shared delivery optics. Situated either 60.4 mm from the collection optics, if passing through one dichroic filter (F_1), or 109.4 mm, if passing through both filters (F_1 and F_2), are the lenses that make up the delivery optics. The pair of lenses that make up the delivery optics are a 1-inch bi-convex lens (D_1, f=75 mm; LB1901; ThorLabs) separated from a 2-inch bi-convex lens (D_2, f=175 mm; LB1607; ThorLabs) by 80 mm. This setup serves to impart approximate collimation to the converging light delivered from the collection optics and provide a final step of beam shaping to create a super-gaussian spot 6 cm from the final lens. As, unlike

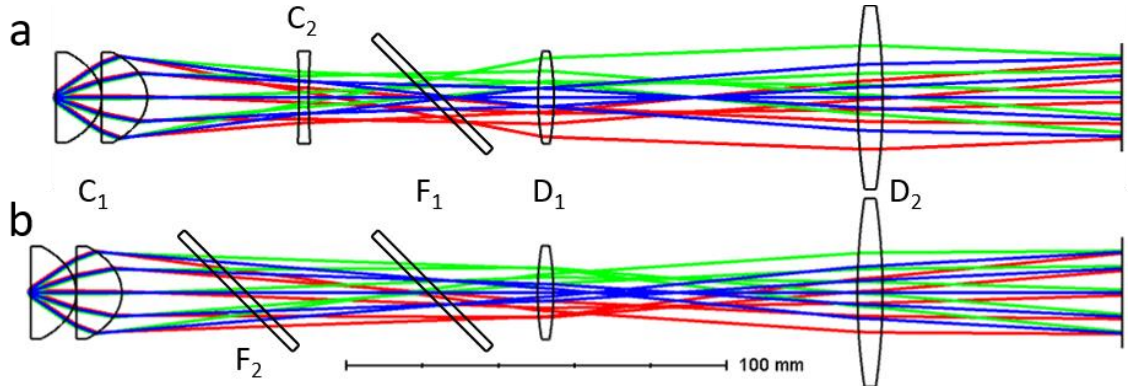

Figure 2.2: Optical designs to generate top-hat intensity profiles. Ray traces showing the collection and beam shaping of divergent LED light into an equal intensity spot while passing through either one dichroic filter (a) or two dichroic filters (b).

with gaussian profiles, super-gaussian intensity profiles are not a free space mode, their intensity profiles change with propagation distance [68]. As the delivery optics are shared and thus cannot be altered, the collection optics must compensate to allow for every super-gaussian to occur at the same location. To accomplish this, the collection optics for the LEDs with a shorter total pathlength, due to interacting with only one dichroic filter (Fig. 2.2a), were altered by adding a bi-concave lens (C_2, f=-200 mm; KBC031; Newport) 40 mm after the aspheric pseudo-doublet.

Characterization of the light distribution from each of the two setups was performed using a beam profiling camera (TaperCamD-UCD23; DataRay Inc.) effective for wavelengths between 350 and 1150 nm. Two-dimensional relative intensity projections were obtained by imaging the beam with an exposure time of 100 ms after passing it through a 1 cm square mask, to fit into the 20 x 15 mm image size of the camera, and a neutral density filter with an OD of 4 to prevent saturation. Profiles of the light distribution were taken diagonally through the square mask to best represent the distribution of the full spot. To account for day-to-day variance, the irradiance of each light source was measured using a photodiode-base power meter before each experiment (Table 2.1).

Photodynamic Therapy Assays

Stock solutions of δ-aminolevulinic acid hydrochloride (ALA; Frontier Biosciences) and the small molecule VU0038882 (‘882) were made in TSB immediately prior to use. Stock solutions containing both ALA and ‘882 were made by combing double concentrated solutions of each. The overnight cultures of *S. aureus* were subcultured 1:10 in either fresh TSB or one of the prepared stock solutions. The subcultures were grown in the dark in a shaking incubator at 37°C for 2 hours to reach exponential growth phase and allow for CPIII

accumulation. After incubation, the subcultures were centrifuged and the resulting bacterial pellets were washed once with ice-cold phosphate-buffered saline to slow growth, recentrifuged and resuspended in PBS at the original subculture volume of 1 mL.

To test the bactericidal effect of a single dose of light, the resuspended subcultures were diluted 1:10 in PBS before transferring 25 μL of the dilution into one well of a black 384-well plate. A 3-well by 3-well area was exposed to the desired light dose, allowing for two pseudo-replicates of each of the four photosensitizer groups (vehicle, ALA, '882, and ALA+'882) to be tested at the same time. The remaining volume of dilution was removed from ambient light and treated as the light-negative, or dark, treatment group. After the light treatment, both the light-exposed and corresponding dark bacteria were serially diluted 1:10, plated on TSA and allowed to grow at 37°C for 20 hours. The final bacterial concentrations were estimated as number of colony-forming units per milliliter (CFU/mL) by counting the number of colonies in the highest dilution with visible growth.

To determine the dose-dependent effects of the applied light, a slightly altered protocol was used. After being washed and resuspended, 200 μL of the subculture were diluted into 1800 μL of PBS before being transferred to a single well of a 12-well plate. While the entire well was illuminated with the chosen light(s), 25 μL were removed at every time point corresponding to the desired light doses. The bacteria were then serially diluted, plated, grown and counted to estimate their concentration.

Monte Carlo Model

Using the Monte Carlo software MCXLAB, a seven-layer skin model was defined based on the work Meglinski and Matcher [69, 70]. This model included separate layers for the stratum corneum, living epidermis, papillary dermis, subpapillary plexus, reticular

dermis, cutaneous plexus, and subcutaneous adipose tissue with thicknesses (d) based on those of an average, healthy adult (Table 2.2) [11, 13]. The absorption (μ_a) and scattering (μ_s) coefficients were defined for each tissue layer between 350 nm and 750 nm with a 1 nm spectral resolution while a constant refractive index (n) and anisotropy (g) were assumed for each layer (Table 2.2) [70]. The optical properties were chosen assuming lightly pigmented skin with a 1% melanin concentration in the living epidermis, corresponding to a Fitzpatrick skin type I or II [71, 72]. This seven-layer depth profile was parallelized into a 4 mm x 4 mm x 3 mm volume with 10 μm cubic voxels. Due to computational limitations, a 3.6 mm diameter disc-shaped light with a top-hat intensity profile was made to illuminate the surface of the skin. Simulations were run using $5x10^8$ photons at each defined wavelength. Using the assumption from PPIX-based PDT for skin cancer, the concentration of accumulated CPIII was assumed to be small enough to not significantly alter the optical properties [73].

Table 2.2: Monte Carlo layers of the skin

	d (μm)	n	g
Layer 1: Stratum Corneum	20	1.50	0.86
Layer 2: Living Epidermis	80	1.34	0.80
Layer 3: Papillary Dermis	150	1.40	0.90
Layer 4: Subpapillary Plexus	80	1.39	0.95
Layer 5: Reticular Dermis	1500	1.40	0.80
Layer 6: Cutaneous Plexus	80	1.38	0.95
Layer 7: Subcutaneous Fat	6000	1.44	0.75

Predicted Light Killing Efficacy in Depth

Following the process outline by LaRochelle *et al.*, the results of the Monte Carlo simulations were used to determine the expected fluence rates of the 395 nm, 565 nm, and 625 nm light sources as a function of depth in the skin [74]. First, the spectral irradiance of

each light source was determined by scaling the normalized intensity spectrum by a constant such that the integral of the scaled spectrum equaled previously measured irradiance values for that LED. The estimated spectral fluence rate at a given depth can then be determined by weighing each spectral irradiance value by the relative spectral transmission that was modeled for that wavelength at the given depth. Thus, the estimated spectral fluence rate at a depth z is:

$$\phi(\lambda, z)\left(\left[{}^{mW}/_{cm^2}\right]/nm\right) = E_{calc}(\lambda, 0) * \phi_{model}(\lambda, z) \quad (1)$$

Where E_{calc} (mW/cm^2) is the calculated spectral irradiance at the surface of the skin and ϕ_{model} ($1/nm$) is the normalized spectral transmission predicted for wavelength λ at depth z by the Monte Carlo model. By integrating this spectrum over its range of wavelengths, the predicted fluence rate can be obtained.

While this calculation does provide the expected fluence rate of each LED as a function of depth in the skin, this value is of little use by itself in predicting the efficacy of light therapy at a given depth. This is because the different spectral components of the LEDs will experience different amounts of attenuation resulting in a distortion of the spectral intensity profile. As CPIII does not absorb all of the applied wavelengths equally, simply using the total fluence rate at a given depth will not provide an accurate prediction of efficacy. To address this, a technique utilized by daylight-PDT was used [74–78].

To address the effectiveness of different white-light sources used in daylight-PDT, these groups utilize an 'effective' fluence rate, $\phi_{eff}(\lambda,z)$, that has shown better correlation with the effectiveness of treatment as compared to true value. The effectiveness of the measure is obtained by weighting the spectral fluence rate by the normalized absorption spectrum of the photosensitizer of interest, which in this case is CPIII. Thus, the CPIII-

weighted, effective fluence rate, $\phi_{eff}(\lambda,z)$, can be calculated as before with:

$$\phi_{eff}(\lambda,z)\left(\left[{}^{mW}/_{cm^2}\right]/nm\right) = E_{calc}(\lambda,0) * \phi_{model}(\lambda,z) * A_{CPIII}(\lambda) \quad (2)$$

Where A_{CPIII} is the normalized absorbance of coproporphyrin III.

For any given treatment time, the CPIII-weighted fluence rate can be used to determine the corresponding total effective light dose. Using the previously measured light dose-dependent light killing effects, converted into CPIII-weighted light doses, log-reductions for *S. aureus* can be predicted at any given depth in the skin. By scaling the time of exposure, predictions can be made on the minimum exposure time required to achieve a 2-log reduction in bacterial concentration at any given depth.

Statistical Analysis

Estimated bacterial concentrations are reported as geometric means ± the geometric standard deviation. The means of each light-treated group were compared to their corresponding light-negative control using a two-tailed t-test, correcting for multiple comparisons with the Holm-Sidak method [79]. As the measured data is assumed to have a log-normal distribution, the measurements were log-transformed prior to analysis to conform to the normal distribution assumption of the Student's t-test.

The results of the light dose-dependent effects are presented as the survival fraction defined as:

$$Survival\ Fraction = {}^{N}/_{N_0} \quad (3)$$

Where N_0 is the number of CFU/mL at time zero (0 J/cm^2) and N is the number of CFU/mL after a given light dose. Survival fractions are reported as geometric means ± the geometric standard deviation. The dose-responses for different treatment groups were compared using

two-way ANOVA and fitted to a logistic function defined as:

$$Y(x) = {}^{L}/_{[1 + e^{-k(x-x_0)}]} \quad (4)$$

Where x_0 is the midpoint of the curve, L is the curve's end value, and k is the steepness of the curve. As the survival fraction values are assumed to have a log-normal distribution, they were log-transformed prior to conform to the normal distribution assumption of ANOVA.

Results

Verification of Top-Hat Intensity Profile

While the original optical setup using the single condenser lens worked to combine the outputs of multiple LEDs, an unforeseen consequence emerged. Although final spot size was large enough to cover the entire 3 x 3 set of wells in the 354-well plate, the samples placed on the outer edges, especially the corners, saw dramatically reduced log-reductions as compared to their corresponding pseudo-replicate. After measuring the intensity profile of the spot on the sample (Fig. 2.3) it was hypothesized that the approximately gaussian distribution was resulting in significantly less light being delivered to the outermost wells in the corners, as compared to the center. The new optical setup addressed this by equalizing the intensity of the light throughout the illumination spot. This proved successful as the measured intensity profiles for each LED used with the new setup demonstrated approximate top-hat intensity profiles (Fig. 2.3). These results confirm that any point within the spot receives approximately the same dose of light.

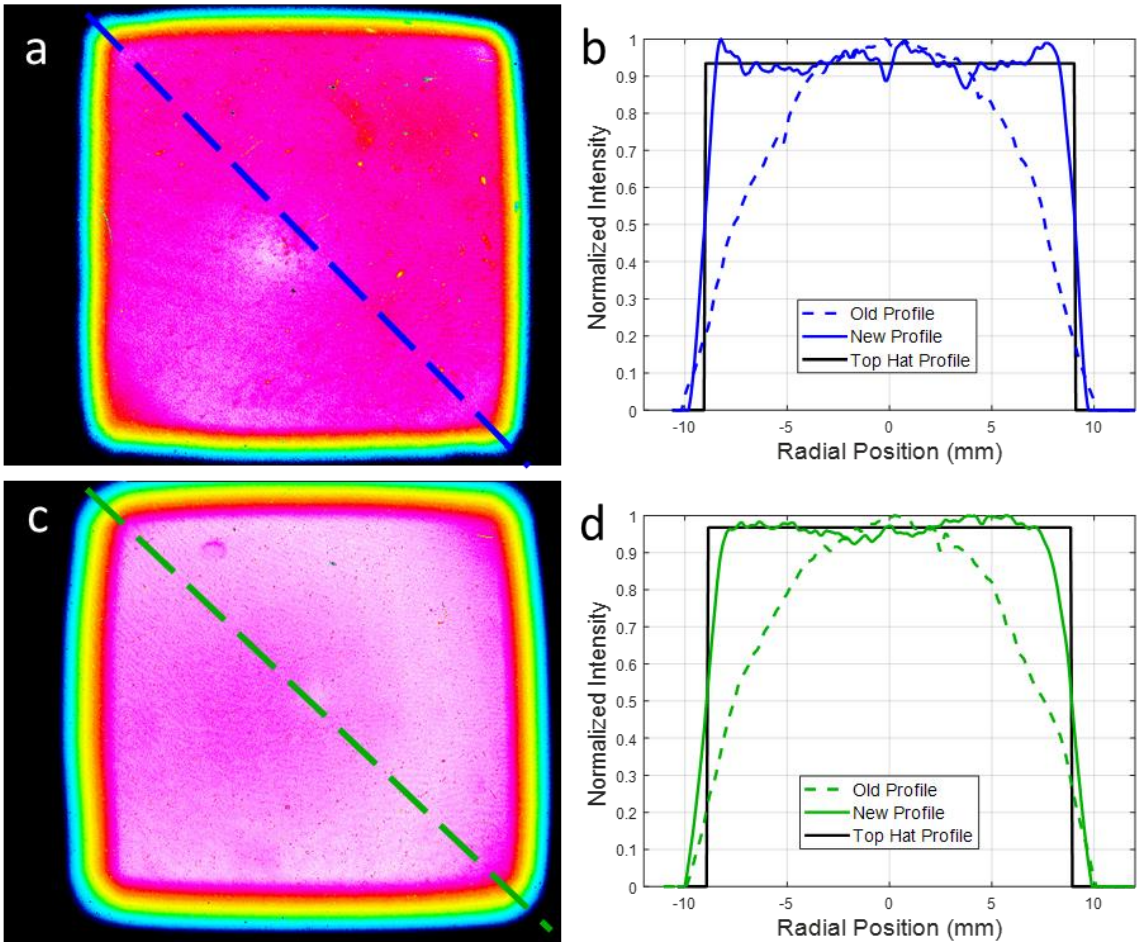

Figure 2.3: Intensity profile measurements. Representative 2-D intensity profiles from the single dichroic filter (a, 395 nm LED) and double dichroic filter (c, 565 nm LED) paths of the new optical setup. Cross-sections from the 395 nm LED (b) and 565 nm LED (d) are compared to those from the old optical setup and a true top-hat profile.

Soret Band Targeted Photodynamic Therapy

To explore the efficacy of targeting the coproporphyrin III Soret band, the single light dose light killing assay was performed using 395 nm LED at a dose of 50 J/cm^2. After a two-hour long subculture with ALA (4 mM), '882 (50 μM), or both, treatment with the 395 nm LED resulted in significant reductions in the viability of USA300 *S. aureus*. Treatment with '882 resulted in the lowest reduction of 2.0 $\log_{10}$-units while ALA treatment provided a 3.8 log-reduction. Treating with a combination of ALA and '882 proved to provide a synergistic photosensitization resulting in a total reduction of 5.2 $\log_{10}$-units in cell viability (Fig. 2.4a).

+ To investigate the sensitivity of correctly targeting the coproporphyrin III Soret band, the bactericidal effects of ALA and the 395 nm LED were compared to that of the 415 nm LED. After a treatment of 4 mM ALA, exposure to 50 J/cm^2 from the 415 nm LED resulted in a reduction of only 0.5 $\log_{10}$-units. While increasing the ALA subculture concentration to 120 mM improved the bactericidal effect of the 415 nm light, resulting in a 1.9 $\log_{10}$-unit reduction, it was still less effective than the 395 nm light after treating with 4 mM of ALA (Fig. 2.4b).

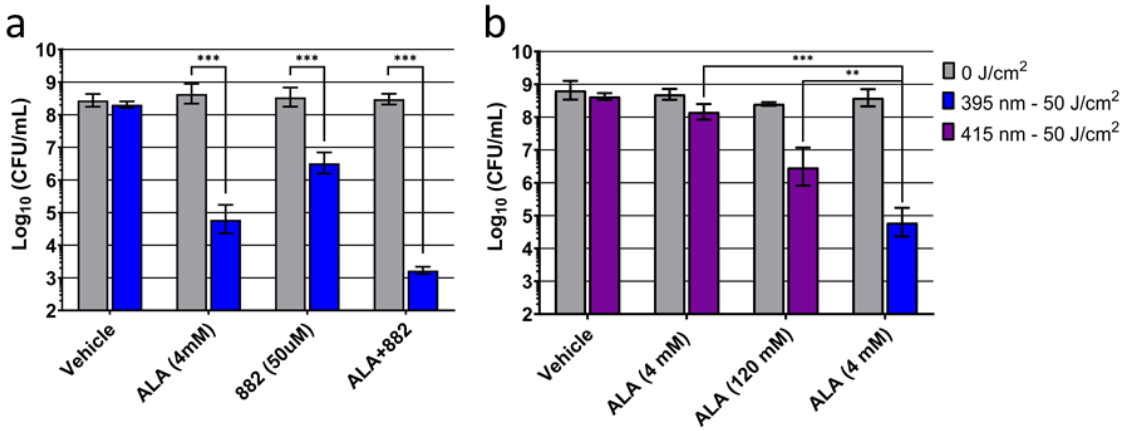

Figure 2.4: Soret band targeted PDT of *S. aureus*. (a) 50 J/cm^2 of 395 nm light provides a significant reduction in *S. aureus* USA300 viability when using both ALA (4 mM) and '882 (50 µM). Combing ALA and '882 provides a synergistic reduction bacterial concentration. (b) 50 J/cm^2 of 415 nm light provides a smaller reduction of *S. aureus* USA300 using either 4 mM or 120 mM ALA as compared to 50 J/cm^2 of 395 nm light and 4 mM ALA. (n=4) ** indicates $p<0.01$ and *** indicates $p<0.001$.

Q-Band Targeted Photodynamic Therapy

The effectiveness of CPIII-aPDT when using wavelengths of light outside of the Soret band was determined by using LEDs whose emitted light corresponded to either two, one, or none of the Q-bands. For each of the tested light sources, the effects of 4 mM ALA, '882 and their combination were determined. As expected, exposure to the 690 nm LED, falling outside of the longest wavelength Q-band, did not exhibit a significant reduction in *S. aureus* in any of the photosensitization groups. This lack of effect persisted even when the applied dose increased to 200 J/cm^2.

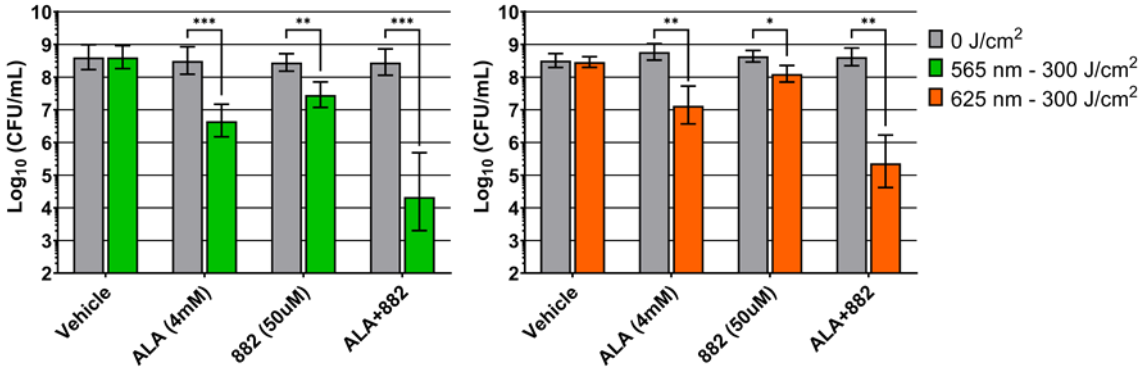

Figure 2.5: Q-band targeted PDT of *S. aureus*. Application of 300 J/cm^2 of either 565 nm or 625 nm light significantly reduces the viability of *S. aureus* USA300 after photosensitization by either 4 mM ALA or 50 μM '882. Combing ALA and '882 provides a synergistic reduction bacterial viability. (n=4) * indicates $p<0.05$, ** indicates $p<0.01$ and *** indicates $p<0.001$.

On the other hand, both the broadband 565 nm LED, corresponding to the central two Q-bands, and the 625 nm LED, corresponding to the last, most red-shifted Q-band, demonstrated that they can induce significant bactericidal effects when large doses of light are used (Fig. 2.5). After exposure to 300 J/cm^2 of 565 nm light, *S. aureus* experienced decreases in viability of 1.8, 1.0, and 4.1 $\log_{10}$-units, corresponding to photosensitization from ALA, '882 and the combination of the two, respectively. Using the same dose of 300 J/cm^2, 625 nm light induced a slightly smaller decrease in *S. aureus* with log reductions ranging from 0.5, for '882 alone, to 3.3 for ALA plus '882.

Dose-Dependent Light Killing

To understand the light dose-response relationship of CPIII-aPDT, the dose-dependent light killing assay was performed using the 395 nm, 565 nm, and 625 nm LEDs and all three photosensitization treatment groups (Fig. 2.6). For the 395 nm LED, measurements were taken between 0 and 50 J/cm^2 while this range was extended out to 500 J/cm^2 for the 565 nm and 625 nm lights. From these results, it was observed that no matter the light source or method of photosensitization, the survival fraction asymptotically

approached some minimum whose value is dependent on the degree of photosensitization. Additionally, the rate at which the minimum survival fraction is reached is dependent on both the wavelength of light used and the degree of photosensitization. This is best represented by the dose-response of '882-treated USA300 exposed to 395 nm light where the maximum reduction in viability is reached after only 40 J/cm^2. Moreover, combinations of lower photosensitization and less efficient, Q-band targeted light demonstrate a lag in the bactericidal effect that results in a minimum required light dose before a reduction in USA300 viability is observed.

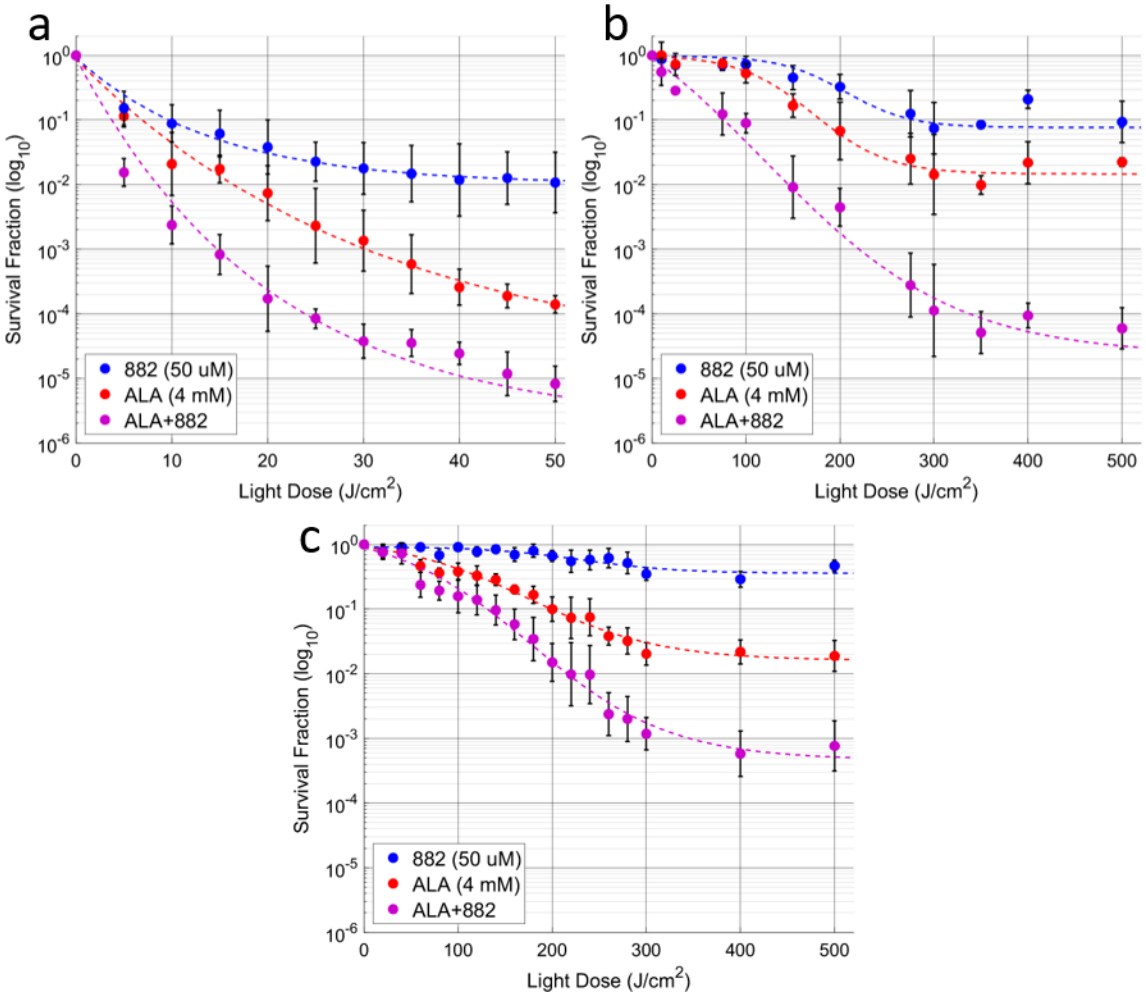

Figure 2.6: Light dose-dependent response of CPIII-aPDT. USA300 photosensitized using ALA, 882 or both exhibit well-defined reductions in cell viability when treated with (a) 395 nm light, (b) 565 nm light, and (c) 625 nm light. Dashed lines represent the logistic function fit to the survival fraction replicates (n=5).

Predicted Efficacy in Depth

To utilize the dose-dependent responses for predicting the expected efficacy of aPDT, it is necessary to have an understanding of how light propagates through the skin. This was achieved by using a seven-layer skin model to simulate the propagation of light with wavelengths between 350 and 750 nm (Fig. 2.7). As expected, it was found that blue light of around 400 nm experiences strong attenuation in the initial layers of the skin, limiting its penetration depth, where the initial intensity has fallen to 1/e, or approximately 37%, of the starting value, to 150 μm. While green and red light experienced less attenuation as compared to blue light, their penetration depths were still limited to 520 μm and 1.2 mm, respectively.

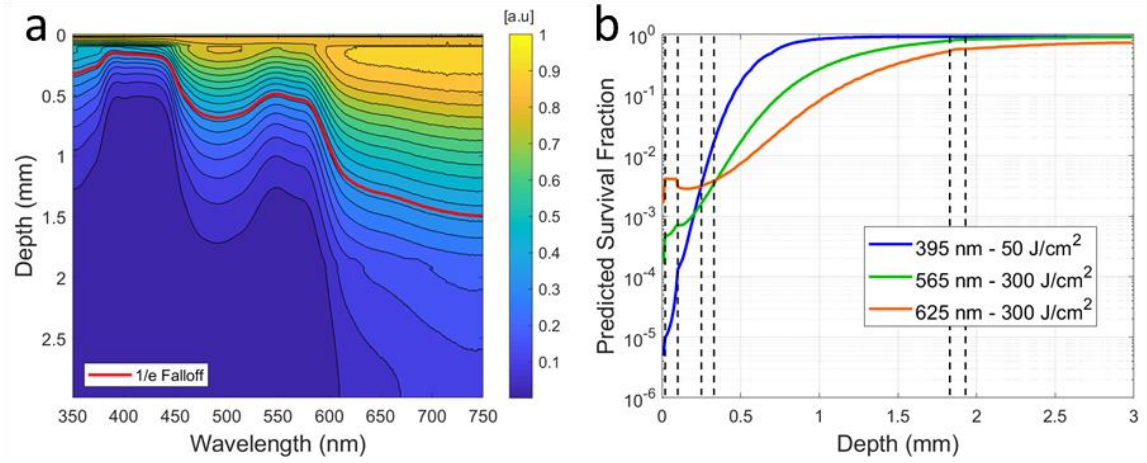

Figure 2.7 Predicted efficacy of CPIII-aPDT in the skin. (a) Fluence rate of 350-750 nm light propagating through the skin normalized to the irradiance at the surface. Black lines indicate a 5 percent change in fluence rate while the red line indicated the 1/e penetration depth. (b) Predicted reduction of cell viability in depth for *S. aureus* USA300 photosensitized using 4 mM ALA and 50 μm '882 before light treatment. Dashed lines indicate the borders between layers of the skin.

Given an applied dose of light on the surface of the skin, this attenuation map can provide the resultant fluence rate for the 395 nm, 565 nm, and 625 nm LEDs at any given depth in the skin. These values can be used in conjunction with the previously measured light dose-dependent responses to predict the efficacy in depth. Given an applied dose of 50 J/cm^2

from the 395 nm LED after inducing photosensitization with 4 mM ALA and 50 μm '882, it was predicted that the reduction in *S. aureus* would drop from over 5 $\log_{10}$-units at the surface to 2 $\log_{10}$-units only 300 μm deep. Despite lower reductions at the surface compared to the 395 nm light, a dose of 300 J/cm^2 applied to the surface of the skin, from either the 565 nm or 625 nm lights, was predicted to provide a 2 $\log_{10}$-unit reduction for a greater depth of the skin, 440 and 560 μm respectively.

Effects of Using Multiple Light Sources

The effects of using two light sources with different wavelengths to activate CPIII-aPDT was initially explored using the single light dose assay. It was found that, for all three photosensitization treatments, when *S. aureus* was simultaneously illuminated with 50 J/cm^2 of 395 nm light and 300 J/cm^2 of 565 nm light, using the illumination scheme 'start'

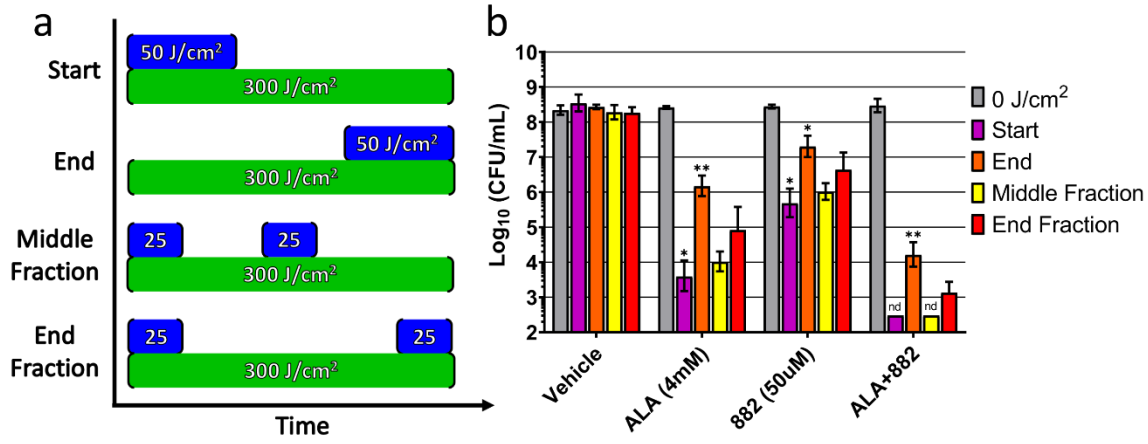

Figure 2.8: Timing-dependent effects of combined light CPIII-aPDT. (a) The effects of distributing the 395 nm light dose (blue) throughout different points of the 565nm dose (green) were tested using the four illumination schemes depicted. (b) The greatest effect of combining 395 and 565 nm light was observed when the entirety of the 395 nm light dose occurred at the beginning of treatment. As more of the 395 nm dose took place later in the treatment, a decrease in efficacy was observed. (n=4) nd indicates no colonies were detected. * indicates $p<0.05$ and ** indicates $p<0.01$ with respect to only 50 J/cm^2 of 395 nm light.

(Fig. 2.8a), a greater reduction in cell viability was obtained. To better understand the mechanisms behind this increase, the 395 nm dose of light was distributed at different points

during the longer 565 nm dose (Fig. 2.8a). It was observed that as more of the 395 nm dose occurred towards the end of the illumination, a smaller improvement in the reduction of cell viability was observed. When the entirety of the 50 J/cm^2 dose occurred at the end of the illumination time, a negative effect was observed as a smaller reduction in *S. aureus* was obtained when compared to the 395 nm LED alone (Fig. 2.8b).

As it was clear that the greatest benefit of this combination occurs when both light sources are used at the beginning of treatment, the dose-dependent light killing assay was used to gain a better picture of the dynamics during this illumination scheme after photosensitization with both 4 mM ALA and 50 µm '882 (Fig. 2.9a). From this, it was observed that the improvement in bacterial reduction begins extremely quickly with the first measured dose (5 J/cm^2 of 395 nm and 7.5 J/cm^2 of 565 nm light) experiencing nearly an entire $\log_{10}$-unit improvement in *S. aureus* reduction as compared to 395 nm light alone. This is despite 7.5 J/cm^2 of 565 nm light only reducing *S. aureus* viability by 0.2 $\log_{10}$-units.

When testing the effects of other combinations of light, it was discovered that despite having no observable effect by itself, the 690 nm LED was able to provide a similar

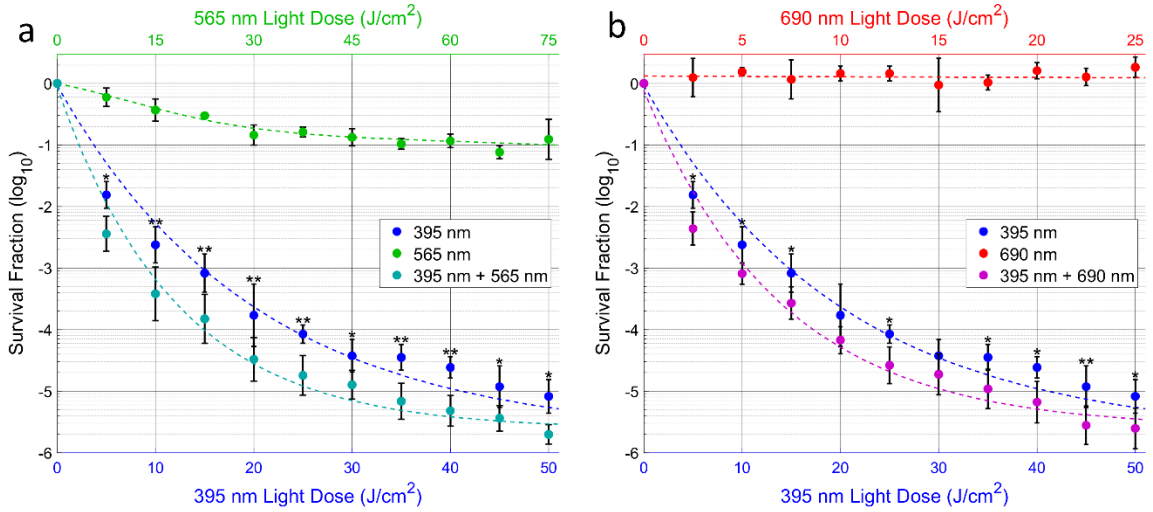

Figure 2.9: Dose-dependent response of combined light CPIII-aPDT. After photosensitization with 4 mM ALA and 50 µM '882, exposure to 395 nm light and either 565 nm light (a) or 690 nm light (b) results in a further reduction in USA300 viability as compared to either light alone. (n=4) * indicates $p<0.05$ and ** indicates $p<0.01$ when comparing the combination therapy and 395 nm light alone.

improvement over using the 395 nm LED alone (Fig. 2.9b). From the results of the dose-dependent assay, it was found that, as with the 565 nm LED, the combination of the 690 and 395 nm LEDs provided an almost immediate increase in performance of 0.5 $\log_{10}$-units that was maintained throughout the entirety of the 395 nm dose. Interestingly, this improvement occurs despite each measurement point only have 5 J/cm^2 of 690 nm light for every 10 J/cm^2 of 395 nm.

Discussion

Skin and soft tissue infection are commonly caused by Gram-positive bacteria with *S. aureus* being the primary pathogen. In recent years, treatment of *S. aureus* skin infections has been complicated by the increase in antibiotic resistant strains present in the population. New strategies are needed that can treat these infections while reducing or eliminating the development of new resistances. Photodynamic therapy is one alternative to antibiotics that we and others have demonstrated as having promise of being able to meet these needs [30, 44, 45, 80].

Recently, the use of endogenous photosensitizers in antimicrobial photodynamic therapy has drastically reduced in favor of various exogenous photosensitizers with recent reviews omitting endogenous photosensitization altogether [42, 45]. This falling out of favor has mostly been due to the lack of specificity and efficacy reported when using ALA to induce photosensitization. However, the recent discovery of the unique heme biosynthesis pathway of Gram-positive bacteria, and it use of coproporphyrin III instead of protoporphyrin IX, has suggested that the previously reported low efficacy may be due to incorrectly targeting the wrong photosensitizer [28]. Additionally, the work by Surdel *et al*. has shown that it is possible to use this unique pathway to specifically target Gram-positive

bacteria [30].

To address these findings, we explored the effectiveness of properly targeting the main absorption peak of CPIII. Using 395 nm light, corresponding to the CPIII Soret band, we obtained significant reductions in *S. aureus* viability regardless of the method of photosensitization. While 4 mM ALA was shown to have a stronger effect as compared to 50 μM '882, this is most likely due to differences in their mechanism of action. ALA floods the heme biosynthesis pathway with the rate-limited precursor effectively by passing the largest check of the pathway. '882, on the other hand, directly upregulates the activity of the CPIII-producing enzyme and thus relies on the normal amounts of precursor molecules that the cell produces, limiting the total amount of CPIII that can accumulate at one time. However, these different mechanisms of action allow ALA and '882 to work synergistically, resulting in a greater accumulation of CPIII and thus a greater reduction in *S. aureus* viability.

In order to achieve the up to 5-log reduction in cell viability that we observed, optimal activation of CPIII is required. This is showcased by the reduced effect observed when using a 415 nm light source representative of the light sources used in previous works testing ALA-PDT in *S. aureus* [66]. Despite using the same amount of ALA and light, the 415 nm light source only provided a 0.5 $\log_{10}$-unit reduction as compared to the 3.8 $\log_{10}$-unit reduction when using 395 nm light. This drastic difference is maintained when the amount of ALA used in the 415 nm treatment is increased to 120 mM. As our results from using the 415 nm LED closely match with those previously reported, it is apparent that the efficacy of using endogenous PDT in Gram-positive bacteria has been drastically underestimated [66].

While we demonstrated that 395 nm light can be used to induce a significant reduction in *S. aureus* viability *in vitro*, blue light around this wavelength has poor

transmission through the skin limiting its usefulness in infections located below the epidermis. Our proposed solution to this issue is to use red-shifted light targeting the Q-bands as they experience less attenuation in the skin. The effectiveness of using this method for CPIII-aPDT was determined by using light sources that target either zero, one, or two Q-bands. As is expected, it was found that using a light not targeting any of the Q-bands resulted in no observable bacterial killing. Additionally, it was observed that when at least one Q-band is targeted a significant bactericidal effect is obtained. However, due to the relatively weaker absorption of the Q-bands, a substantially larger dose of light is required as compared to targeting the Soret band.

When exploring the light-dose dependent effects of the three light sources, a couple of interesting observations were made. First, it was found that, for all treatment combinations, the reduction of bacterial viability would not decrease past a certain point despite the addition of more light. As PDT requires three main components to work, light, PS, and oxygen, and excess light was supplied, either oxygen or the PS must be acting as a limiting factor. While it is unknown which of the two is truly limited, this behavior is most likely due to photobleaching or photodamage of CPIII as the experimental system could freely exchange oxygen with the environment. The second interesting observation that was made was that all of the combinations using Q-band targeted light, except for the ALA plus ‘882 group treated with 565 nm light, experienced a delay in effect at low light doses with minimal to no bacterial killing observed. While the reason behind this behavior has also not been confirmed, it is reasonable to assume that it is due the rate of singlet oxygen production being too low to completely overcome the natural antioxidants of the bacteria requiring the amount of singlet oxygen to accumulate until lethal levels are achieved. This is supported by the fact that the treatment combination of ALA, ‘882 and 565 nm light, the most effective

treatment outside of using the 395 nm light source, did not experience this delay in effect.

As targeting both the Soret band and the Q-bands each have their own disadvantages, it was unknown which would be more effective at treating infections at different depths of the skin. To better predict the efficacy of using these different light sources to treat a real infection at some depth in the skin, the results of a Monte Carlo simulation were combined with the previous dose-dependent responses. However, these predictions are unverified and are reliant on a number of different assumptions including the validity of the Monte Carlo simulation, that bacteria in the skin could be photosensitized to the same degree as the *in vitro* experiments, and that the bacteria will have the same access to oxygen during PDT.

If we hold these assumptions to be true, we can use this predictive model to determine the requirements for treating a *S. aureus* skin infection in a best-case scenario. From the model, it was found that despite the high absorption of blue light by the skin, the high efficiency of using 395 nm light to activate CPIII-aPDT acts as a counterbalance, allowing for a surface dose of only 60 J/cm^2 to provide a 2 $\log_{10}$-unit reduction 330 μm deep in the skin (Table 2.3). However, the required dose rises exponentially when targeting any deeper. While this could be done in theory, increasing the light dose of highly absorbed wavelengths will result in photothermal damage of the tissue. Although larger doses of light are also required for the 565 nm and 625 nm lights to exhibit an effect in depth, the rate of increase is less dramatic due to reduced attenuation by the skin. The is best showcased by the 625 nm light. While it would take a surface dose of over 250 J/cm^2 to achieve a 2-log reduction 20 μm into the skin, it would take less than double that amount at 466 J/cm^2 to obtain the same level of bacterial reduction a full millimeter into skin. Proper application of this predictive model would allow for the ideal light source to be chosen to treat a given infection given its depth of localization.

Table 2.3: Applied light dose (J/cm^2) for a 2-log bacterial reduction in depth

	395 nm	565 nm	625 nm
20 µm	10.5	174.1	258.1
100 µm	19.0	185.9	241.4
250 µm	37.7	214.7	244.3
330 µm	58.1	244.4	253.4
500 µm	147.4	335.7	285.0
1000 µm	2,255.7	963.4	465.9
1910 µm	>300,000	9,435.1	1,615.6
3000 µm	>6,000,000	42,420.4	3,158.5

While the 565 nm and 625 nm lights are predicted to be more effective in depth as compared to using 395 nm light, they have demonstrated a lower maximum capacity for bacterial reduction at the same level of photosensitization. It was hypothesized that by simultaneously using 395 nm light and Q-band targeted light, strong killing at the surface could be maintained while improving the overall effects in depth. When testing these combinations together *in vitro*, it was found that a simultaneous dose of 50 J/cm^2 of 395 nm light and 300 J/cm^2 of 565 nm light resulted in an improvement in the reduction of *S. aureus* viability as compared to either light alone. This improvement appears to begin immediately during treatment as a significant increase in reduction observed at the earliest measure light dose. Additionally, it was determined that this effect must occur at the beginning of the illumination period as when the 395 nm light dose is moved to the end, results similar to those of the 565 nm light alone are obtained. This indicates that the improvement may be caused by an increase in the rate of singlet oxygen production. By quickly reaching the lethal threshold of singlet oxygen, significant levels of bacterial killing are achieved at a lower dose and that improvement is carried throughout the rest of the dose.

What was more surprising was that this improvement was not limited to using one of the Q-band targeted light sources as using the 690 nm light produced a similar improvement.

albeit weaker, However, this difference may have been due to the low irradiance of the 690 nm LED limiting how much could be applied during the 395 nm light dose. As the 690 nm light does not target an absorption of CPIII, it is unlikely causing a direct increase in singlet oxygen production indicating that another mechanism may be occurring. A better understanding of the process underpinning this improvement could lead to new methods of increasing antimicrobial PDT efficacy.

CHAPTER 3

CONCLUSIONS AND FUTURE DIRECTIONS

Optimal targeting of the main absorption peak, or Soret band, of coproporphyrin III was found to improve endogenous photodynamic therapy of *Staphylococcus aureus* as compared to previously reported results. Additionally, it was found that significant reductions in bacterial viability can be obtained by targeting the minor absorption peaks, or Q-bands, of CPIII, provided that a large enough dose of light is supplied. It was predicted that the use of these different wavelengths would be required to optimally treat infections localized at different depths in the skin, with blue light working better close to the surface and red light working better deep in the skin. It was also discovered that simultaneously using multiple light sources of different wavelengths induces a greater reduction in the viability of *S. aureus* as compared to using either one alone. These results suggest that endogenous photodynamic therapy has the potential to be further developed into a valid treatment of skin and soft tissue infections caused by Gram-positive bacteria.

Identification of Limiting Factors

While determining the dose-dependent effects of different light sources and methods of photosensitization, it was determined that the maximum reduction in *S. aureus* was being limited by either the amount of photosensitizer or molecular oxygen, two of the three main components required in PDT. Determining what is acting as the limiting factor would inform future work what additional steps are necessary to improve the efficacy of CPIII-aPDT. Using fluorescence to measure the porphyrin photobleaching dynamics has become a common method of evaluating the dosimetry of PPIX-PDT [81]. As CPIII is a porphyrin

similar to PPIX, the same measurement could be made and compared to dose-dependent responses. If the limitation is truly due to degradation of the photosensitizers, a correlation between the two should be observed. If this assumption is proven to be true, re-photosensitizing the area after a certain dose of light should be able to further improve the performance of CPIII-aPDT.

To determine if oxygen is the major limiting factor, measuring dose dependent light killing in environments with controlled oxygen levels could be performed. If performing the experiment under increased oxygen results in reduction or elimination of the observed limit while decreased oxygen increases the limit, it can be concluded that oxygen is the dominant limiting factor. While this information would be harder to implement in improving CPIII-aPDT, methods like heating the skin to induce vascular dilation could result enough extra oxygen being delivered to the skin to result in an improvement.

Improvement of Predictive Model

As mentioned previously, the model used in this work to predict the how effective the tested light sources would be in treating infections localized to different depths of the skin relied on a number of assumptions. The first of these assumptions was that the results of the Monte Carlo simulation in the seven-layer skin model accurately predicted the behavior of light passing through the skin. To be more confident in the predictive model, these results should be verified against actual transmission measurements through skin taken using a spectrophotometer. While the behavior within the skin could not be confirmed, the relative amount of light passing through some thickness of skin could be verified. Additionally, damaged and infected skin will have different optical properties as compared to healthy skin due to blood, pus, and erythema altering the relative composition.

Determining and using the optical properties of infected skin would help to better predict how the light will travel in depth.

Another assumption that was made was that the effects of CPIII-aPDT in the skin would be similar to the results obtain *in vitro*. As the skin is a much more complex environment than the benchtop, it would be better if the dose-response data used in the model was based on *in vivo* results. A mouse model of a superficial skin infection would be the ideal method to determine the effects of CPIII-aPDT in the skin with minor interference from absorption by the skin [30].

Once the predictive model has become more reliable, there are a couple other features that could be implemented to improve its performance [74]. The first would be modeling the accumulation of CPIII overtime after application of ALA or ‘882. By understanding the degree of photosensitization achieved at different depths in the skin, more accurate predictions of the bacterial reduction can be made. Additionally, modeling the photobleaching of CPIII, and thus the removal of viable photosensitizer, would help gauge the correct fluence rate required to achieve an optimal performance.

Determine Light Combination Mechanism

While this work discovered that light not targeting an absorption peak of CPIII can provide an improvement in light killing when used in conjunction with light targeting the Soret band, there is a lack of understanding of how this occurs. First, it should be confirmed that 690 nm light increases the production of singlet oxygen indicating that it is interacting with CPIII in some manner. Measurement of singlet oxygen can be done optically either through the direct measurement of the phosphorescent light releases when singlet oxygen returns to the triplet ground state or by using a dye, like singlet oxygen sensor green, that

only fluoresces when it has been oxidized by singlet oxygen.

Once an increase in singlet oxygen has been confirmed, the mechanism behind the increase should be investigated. First, it should be confirmed that 690 nm light alone does not induce light killing. This could be done by using a Gram-positive species that has been shown to be high susceptible to photodynamic therapy, like *Propionibacterium acnes*, or a chemical like potassium iodide that has shown to potentiate the effects of antimicrobial PDT [30, 82]. After confirmation, the cause of the increased singlet oxygen production would need to be determined. One possibility that would need to be examined is the potential of CPIII forming a photoproduct in response to 395 nm light that, similar to the photoproduct of PPIX, has further red-shifted absorption bands [83]. If these absorption bands are shifted enough, they may absorb 690 nm light. Correctly determining this mechanism could allow for the development of a new technique that further improves CPIII-aPDT in treating Gram-positive bacterial skin infections.

BIBLIOGRAPHY

[1] M. Basra and M. Shahrukh, "Burden of Skin Diseases," *Expert Rev. Pharmacoecon. Outcomes Res.*, vol. 9, no. 3, pp. 271–283, 2009.

[2] L. Tognetti *et al.*, "Bacterial skin and soft tissue infections: Review of the epidemiology, microbiology, aetiopathogenesis and treatment: A collaboration between dermatologists and infectivologists," *J. Eur. Acad. Dermatology Venereol.*, vol. 26, no. 8, pp. 931–941, 2012.

[3] K. Chiller, B. A. Selkin, and G. J. Murakawa, "Skin Microflora and Bacterial Infections of the Skin," *J. Investig. Dermatology Symp. Proc.*, vol. 6, no. 3, pp. 170–174, Dec. 2001.

[4] V. Ki and C. Rotstein, "Bacterial skin and soft tissue infections in adults: A review of their epidemiology, pathogenesis, diagnosis, treatment and site of care," *Can.J.Infect.Dis.Med.Microbiol.*, vol. 19, no. 1712–9532 (Print), pp. 173–184, 2008.

[5] A. F. Cardona and S. E. Wilson, "Skin and Soft-Tissue Infections: A Critical Review and the Role of Telavancin in Their Treatment," *Clin. Infect. Dis.*, vol. 61, no. Suppl 2, pp. S69–S78, 2015.

[6] M. S. Dryden, "Skin and soft tissue infection: microbiology and epidemiology," *Int. J. Antimicrob. Agents*, vol. 34, no. SUPPL. 1, pp. S2–S7, 2009.

[7] M. J. DiNubile and B. A. Lipsky, "Complicated infections of skin and skin structures: When the infection is more than skip deep," *J. Antimicrob. Chemother.*, vol. 53, no. SUPPL. 2, pp. 37–50, 2004.

[8] N. Kaushik, G. G. A. Pujalte, and S. T. Reese, "Superficial fungal infections," *Prim. Care - Clin. Off. Pract.*, vol. 42, no. 14, pp. 501–516, 2015.

[9] A. L. Cogen, V. Nizet, and R. L. Gallo, "Skin microbiota: a source of disease or defence?," *Br. J. Dermatol.*, vol. 158, no. 3, pp. 442–55, Mar. 2008.

[10] F. Ibrahim, T. Khan, and G. G. A. Pujalte, "Bacterial Skin Infections," *Prim. Care - Clin. Off. Pract.*, vol. 42, no. 4, pp. 485–499, 2015.

[11] J. A. McGrath, R. A. J. Eady, and F. M. Pope, "Anatomy and Organization of Human Skin," in *Rook's Textbook of Dermatology*, Malden, Massachusetts, USA: Blackwell Publishing, Inc., pp. 45–128.

[12] S. H. Lee, S. K. Jeong, and S. K. Ahn, "An update of the defensive barrier function of skin.," *Yonsei Med. J.*, vol. 47, no. 3, pp. 293–306, Jun. 2006.

[13] A. Rook and T. Burns, *Rook's textbook of dermatology*. Wiley-Blackwell, 2010.

[14] G. Pontrelli and L. Simon, "The Choice of a Performance Indicator of Release in Transdermal Drug Delivery Systems," Springer, Cham, 2018, pp. 49–64.

[15] S. Rajan, "Skin and soft-tissue infections: Classifying and treating a spectrum,"

Cleve. Clin. J. Med., vol. 79, no. 1, pp. 57–66, 2012.

[16] M. J. Sladden and G. a Johnston, "Clinical review Common skin infections in children," *Br. Med. J.*, vol. 329, no. box 1, pp. 95–99, 2004.

[17] K. T. Clebak and M. A. Malone, "Skin Infections," *Prim. Care - Clin. Off. Pract.*, vol. 45, no. 3, pp. 433–454, 2018.

[18] E. A. Grice, "The skin microbiome: potential for novel diagnostic and therapeutic approaches to cutaneous disease.," *Semin. Cutan. Med. Surg.*, vol. 33, no. 2, pp. 98–103, 2014.

[19] S. Laube, "Skin infections and ageing," *Ageing Res. Rev.*, vol. 3, no. 1, pp. 69–89, 2004.

[20] L. J. Eron, B. A. Lipsky, D. E. Low, D. Nathwani, A. D. Tice, and G. A. Volturo, "Managing skin and soft tissue infections: expert panel recommendations on key decision points," *J. Antimicrob. Chemother.*, vol. 52, no. 90001, p. 3i–17, 2003.

[21] D. L. Stevens *et al.*, "Practice guidelines for the diagnosis and management of skin and soft tissue infections: 2014 update by the infectious diseases society of America.," *Clin. Infect. Dis.*, 2014.

[22] P. Ramdass, S. Mullick, and H. F. Farber, "Viral Skin Diseases," *Prim. Care - Clin. Off. Pract.*, vol. 42, no. 4, pp. 517–567, 2015.

[23] M. Fazli *et al.*, "Nonrandom distribution of *Pseudomonas aeruginosa* and *Staphylococcus aureus* in chronic wounds," *J. Clin. Microbiol.*, vol. 47, no. 12, pp. 4084–4089, 2009.

[24] T. Beveridge, "Use of the Gram stain in microbiology," *Biotech. Histochem.*, vol. 76, no. 3, pp. 111–118, Jan. 2001.

[25] O. Schneewind and D. M. Missiakas, "Protein secretion and surface display in Gram-positive bacteria," *Philos. Trans. R. Soc. B Biol. Sci.*, vol. 367, no. 1592, pp. 1123–1139, 2012.

[26] C. Danne and S. Dramsi, "Pili of Gram-positive bacteria: Roles in host colonization," *Res. Microbiol.*, vol. 163, no. 9–10, pp. 645–658, 2012.

[27] T. R. D. Costa *et al.*, "Secretion systems in Gram-negative bacteria: structural and mechanistic insights," *Nat. Rev. Microbiol.*, vol. 13, no. 6, pp. 343–359, 2015.

[28] H. A. Dailey, S. Gerdes, T. A. Dailey, J. S. Burch, and J. D. Phillips, "Noncanonical coproporphyrin-dependent bacterial heme biosynthesis pathway that does not use protoporphyrin," *Proc. Natl. Acad. Sci.*, vol. 112, no. 7, pp. 2210–2215, 2015.

[29] J. E. Choby and E. P. Skaar, "Heme Synthesis and Acquisition in Bacterial Pathogens," *J. Mol. Biol.*, vol. 428, no. 17, pp. 3408–3428, 2016.

BIBLIOGRAPHY

[30] M. C. Surdel *et al.*, "Antibacterial photosensitization through activation of coproporphyrinogen oxidase," *Proc. Natl. Acad. Sci.*, vol. 114, no. 32, pp. E6652–E6659, 2017.

[31] G. J. Moet, R. N. Jones, D. J. Biedenbach, M. G. Stilwell, and T. R. Fritsche, "Contemporary causes of skin and soft tissue infections in North America, Latin America, and Europe: Report from the SENTRY Antimicrobial Surveillance Program (1998–2004)," *Diagn. Microbiol. Infect. Dis.*, vol. 57, no. 1, pp. 7–13, Jan. 2007.

[32] K. Gjødsbøl, J. J. Christensen, T. Karlsmark, B. Jørgensen, B. M. Klein, and K. A. Krogfelt, "Multiple bacterial species reside in chronic wounds: a longitudinal study," vol. 3, no. 3, pp. 225–231, 2006.

[33] E. Banin, D. Hughes, and O. P. Kuipers, "Editorial: Bacterial pathogens, antibiotics and antibiotic resistance," *FEMS Microbiol. Rev.*, vol. 41, no. 3, pp. 450–452, 2017.

[34] M. Frieri, K. Kumar, and A. Boutin, "Antibiotic resistance," *J. Infect. Public Health*, vol. 10, no. 4, pp. 369–378, 2017.

[35] A. H. Holmes *et al.*, "Understanding the mechanisms and drivers of antimicrobial resistance," *Lancet*, vol. 387, no. 10014, pp. 176–187, 2016.

[36] J. M. A. Blair, M. A. Webber, A. J. Baylay, D. O. Ogbolu, and L. J. V Piddock, "Molecular mechanisms of antibiotic resistance," *Nat. Rev. Microbiol.*, vol. 13, no. 1, pp. 42–51, 2015.

[37] V. K. Sharma, N. Johnson, L. Cizmas, T. J. McDonald, and H. Kim, "A review of the influence of treatment strategies on antibiotic resistant bacteria and antibiotic resistance genes," *Chemosphere*, vol. 150, pp. 702–714, 2016.

[38] M. Otto, "Community-associated MRSA: What makes them special?," *Int. J. Med. Microbiol.*, vol. 303, no. 6–7, pp. 324–330, 2013.

[39] E. Martens and A. L. Demain, "The antibiotic resistance crisis, with a focus on the United States," *J. Antibiot. (Tokyo).*, vol. 70, no. 5, pp. 520–526, 2017.

[40] K. T. Bæk *et al.*, "β-Lactam resistance in methicillin-resistant *Staphylococcus aureus* USA300 is increased by inactivation of the ClpXP protease.," *Antimicrob. Agents Chemother.*, vol. 58, no. 8, pp. 4593–603, Aug. 2014.

[41] W. A. McGuinness, N. Malachowa, and F. R. DeLeo, "Vancomycin Resistance in *Staphylococcus aureus* .," *Yale J. Biol. Med.*, vol. 90, no. 2, pp. 269–281, 2017.

[42] N. Kashef and M. R. Hamblin, "Can microbial cells develop resistance to oxidative stress in antimicrobial photodynamic inactivation?," *Drug Resist. Updat.*, vol. 31, pp. 31–42, Mar. 2017.

BIBLIOGRAPHY

[43] Z. Huang, "A Review of Progress in Clinical Photodynamic Therapy," *Technol. Cancer Res. Treat.*, vol. 4, no. 3, pp. 283–293, Jun. 2005.

[44] M. R. Hamblin and T. Hasan, "Photodynamic therapy: a new antimicrobial approach to infectious disease?," *Photochem. Photobiol. Sci.*, vol. 3, no. 5, p. 436, Apr. 2004.

[45] F. Cieplik *et al.*, "Antimicrobial photodynamic therapy as an adjunct for treatment of deep carious lesions—A systematic review," *Photodiagnosis Photodyn. Ther.*, vol. 18, pp. 54–62, Jun. 2017.

[46] P. Calzavara-Pinton, M. Venturini, and R. Sala, "Photodynamic therapy: update 2006 Part 1: Photochemistry and photobiology," *J. Eur. Acad. Dermatology Venereol.*, vol. 21, no. 3, pp. 293–302, Mar. 2007.

[47] C. A. Robertson, D. H. Evans, and H. Abrahamse, "Photodynamic therapy (PDT): A short review on cellular mechanisms and cancer research applications for PDT," *J. Photochem. Photobiol. B Biol.*, vol. 96, no. 1, pp. 1–8, Jul. 2009.

[48] H. Abrahamse and M. R. Hamblin, "New photosensitizers for photodynamic therapy.," *Biochem. J.*, vol. 473, no. 4, pp. 347–64, Feb. 2016.

[49] K. Apel and H. Hirt, "REACTIVE OXYGEN SPECIES: Metabolism, Oxidative Stress, and Signal Transduction," *Annu. Rev. Plant Biol.*, vol. 55, no. 1, pp. 373–399, Jun. 2004.

[50] A. P. Castano, T. N. Demidova, and M. R. Hamblin, "Mechanisms in photodynamic therapy: part one—photosensitizers, photochemistry and cellular localization," *Photodiagnosis Photodyn. Ther.*, vol. 1, no. 4, pp. 279–293, Dec. 2004.

[51] B. Valeur, *Molecular Fluorescence Principles and Applications 2001*. 2001.

[52] M. Tim, "Strategies to optimize photosensitizers for photodynamic inactivation of bacteria," *J. Photochem. Photobiol. B Biol.*, vol. 150, pp. 2–10, Sep. 2015.

[53] S. M. Yoo and S. Y. Lee, "Optical Biosensors for the Detection of Pathogenic Microorganisms," *Trends Biotechnol.*, vol. 34, no. 1, pp. 7–25, Jan. 2016.

[54] F. Berthiaume, S. R. Reiken, M. Toner, R. G. Tompkins, and M. L. Yarmush, "Antibody-targeted Photolysis of Bacteria In Vivo," *Nat. Biotechnol.*, vol. 12, no. 7, pp. 703–706, Jul. 1994.

[55] M. Bhatti, A. MacRobert, B. Henderson, P. Shepherd, J. Cridland, and M. Wilson, "Antibody-targeted lethal photosensitization of *Porphyromonas gingivalis*.," *Antimicrob. Agents Chemother.*, vol. 44, no. 10, pp. 2615–8, Oct. 2000.

[56] L. M. Baltazar, A. Ray, D. A. Santos, P. S. Cisalpino, A. J. Friedman, and J. D. Nosanchuk, "Antimicrobial photodynamic therapy: An effective alternative approach to control fungal infections," *Front. Microbiol.*, vol. 6, no. MAR, pp. 1–

11, 2015.

[57] M. Biesaga, K. Pyrzyńska, and M. Trojanowicz, "Porphyrins in analytical chemistry. A review," *Talanta*, vol. 51, no. 2, pp. 209–224, 2000.

[58] U. Schmidt-Erfurth and T. Hasan, "Mechanisms of Action of Photodynamic Therapy with Verteporfin for the Treatment of Age-Related Macular Degeneration," *Surv. Ophthalmol.*, vol. 45, no. 3, pp. 195–214, Nov. 2000.

[59] P. Ponka, "Cell biology of heme," *Am. J. Med. Sci.*, vol. 318, no. 4, pp. 241–256, 1999.

[60] H. A. Dailey *et al.*, "Prokaryotic Heme Biosynthesis: Multiple Pathways to a Common Essential Product," *Microbiol. Mol. Biol. Rev.*, vol. 81, no. 1, pp. e00048-16, 2017.

[61] L. A. Mike *et al.*, "Activation of heme biosynthesis by a small molecule that is toxic to fermenting *Staphylococcus aureus*," *Proc. Natl. Acad. Sci.*, vol. 110, no. 20, pp. 8206–8211, May 2013.

[62] L. B. Josefsen and R. W. Boyle, "Photodynamic Therapy and the Development of Metal-Based Photosensitisers," *Met. Based. Drugs*, vol. 2008, pp. 1–23, 2008.

[63] M. Gouterman, "Spectra of porphyrins," *J. Mol. Spectrosc.*, vol. 6, pp. 138–163, 1961.

[64] Y. Nitzan, M. Salmon-Divon, E. Shporen, and Z. Malik, "ALA induced photodynamic effects on Gram positive and negative bacteria," *Photochem. Photobiol. Sci.*, 2004.

[65] X. Li *et al.*, "Effects of 5-aminolevulinic acid–mediated photodynamic therapy on antibiotic-resistant staphylococcal biofilm: an in vitro study," *J. Surg. Res.*, vol. 184, no. 2, pp. 1013–1021, Oct. 2013.

[66] K. Morimoto *et al.*, "Photodynamic therapy using systemic administration of 5-aminolevulinic acid and a 410-nm wavelength light-emitting diode for methicillin-resistant *Staphylococcus aureus*-infected ulcers in mice," *PLoS One*, vol. 9, no. 8, pp. 1–8, 2014.

[67] G. J. Moran *et al.*, "Methicillin-Resistant *S. aureus* Infections among Patients in the Emergency Department," *N. Engl. J. Med.*, vol. 355, no. 7, pp. 666–674, Aug. 2006.

[68] A. A. Tovar, "Propagation of flat-topped multi-Gaussian laser beams," *J. Opt. Soc. Am. A*, vol. 18, no. 8, p. 1897, Aug. 2001.

[69] Q. Fang and D. A. Boas, "Monte Carlo Simulation of Photon Migration in 3D Turbid Media Accelerated by Graphics Processing Units," *Opt. Express*, vol. 17, no. 22, p. 20178, Oct. 2009.

[70] I. V Meglinski and S. J. Matcher, “Quantitative assessment of skin layers absorption and skin reflectance spectra simulation in the visible and near-infrared spectral regions,” *Physiol. Meas.*, vol. 23, no. 4, pp. 741–753, Nov. 2002.

[71] T. B. Fitzpatrick, “The Validity and Practicality of Sun-Reactive Skin Types I Through VI,” *Arch. Dermatol.*, vol. 124, no. 6, p. 869, Jun. 1988.

[72] H. Lu, C. Edwards, S. Gaskell, A. Pearse, and R. Marks, “Melanin content and distribution in the surface corneocyte with skin phototypes,” *Br. J. Dermatol.*, vol. 135, no. 2, pp. 263–267, Aug. 1996.

[73] R. M. Valentine, C. T. A. Brown, H. Moseley, S. Ibbotson, and K. Wood, “Monte Carlo modeling of in vivo protoporphyrin IX fluorescence and singlet oxygen production during photodynamic therapy for patients presenting with superficial basal cell carcinomas,” *J. Biomed. Opt.*, vol. 16, no. 4, p. 048002, 2011.

[74] E. P. M. LaRochelle, K. Marra, R. E. LeBlanc, M. S. Chapman, E. V. Maytin, and B. W. Pogue, “Modeling PpIX effective light fluence at depths into the skin for PDT dose comparison,” *Photodiagnosis Photodyn. Ther.*, vol. 25, pp. 425–435, Mar. 2019.

[75] S. R. Wiegell, J. Heydenreich, S. Fabricius, and H. C. Wulf, “Continuous ultra-low-intensity artificial daylight is not as effective as red LED light in photodynamic therapy of multiple actinic keratoses,” *Photodermatol. Photoimmunol. Photomed.*, vol. 27, no. 6, pp. 280–285, Dec. 2011.

[76] S. R. Wiegell *et al.*, “Daylight photodynamic therapy for actinic keratosis: an international consensus,” *J. Eur. Acad. Dermatology Venereol.*, vol. 26, no. 6, pp. 673–679, Jun. 2012.

[77] P. O’Mahoney, M. Khazova, M. Higlett, T. Lister, S. Ibbotson, and E. Eadie, “Use of illuminance as a guide to effective light delivery during daylight photodynamic therapy in the U.K.,” *Br. J. Dermatol.*, vol. 176, no. 6, pp. 1607–1616, Jun. 2017.

[78] L. Spelman *et al.*, “Treatment of face and scalp solar (actinic) keratosis with daylight-mediated photodynamic therapy is possible throughout the year in Australia: Evidence from a clinical and meteorological study,” *Australas. J. Dermatol.*, vol. 57, no. 1, pp. 24–28, Feb. 2016.

[79] S. Holm, “A Simple Sequentially Rejective Multiple Test Procedure,” *Scand. J. Stat.*, vol. 6, no. 2, pp. 65–70, 1979.

[80] G. B. Kharkwal, S. K. Sharma, Y.-Y. Huang, T. Dai, and M. R. Hamblin, “Photodynamic therapy for infections: Clinical applications,” *Lasers Surg. Med.*, vol. 43, no. 7, pp. 755–767, Sep. 2011.

[81] C. Sheng, P. Jack Hoopes, T. Hasan, and B. W. Pogue, “Photobleaching-based Dosimetry Predicts Deposited Dose in ALA-PpIX PDT of Rodent Esophagus,”

Photochem. Photobiol., vol. 83, no. 3, pp. 738–748, May 2007.

[82] D. Vecchio *et al.*, "Bacterial photodynamic inactivation mediated by methylene blue and red light is enhanced by synergistic effect of potassium iodide.," *Antimicrob. Agents Chemother.*, vol. 59, no. 9, pp. 5203–12, Sep. 2015.

[83] L. Ma, S. Bagdonas, and J. Moan, "The photosensitizing effect of the photoproduct of protoporphyrin IX," *J. Photochem. Photobiol. B Biol.*, vol. 60, no. 2–3, pp. 108–113, Jul. 2001.